

Resonant Cavities and Waveguides in the Ionosphere and Atmosphere

R. L. Lysak, University of Minnesota

A. Yoshikawa, Kyushu University

Abstract

The strong inhomogeneities in plasma parameters in the ionosphere and adjacent regions can trap waves in the upper end of the ULF range (Pc1/Pi1). The topside ionosphere is characterized by a rapidly increasing Alfvén speed with a scale height the order of 1000 km. Shear mode Alfvén waves in this region can be partially trapped at frequencies in the 0.1-1.0 Hz range. The same structure can trap fast mode compressional waves in this frequency band. Since these waves can propagate across magnetic field lines, this structure constitutes a waveguide in which energy can propagate at speeds comparable to the Alfvén speed, typically the order of 1000 km/s. Hall effects in the ionosphere couple these two wave modes, so that the introduction of a field-aligned current by means of a shear mode Alfvén wave can excite compressional waves that can propagate in the waveguide. In the limit of infinite ionospheric conductivity, these waves are isolated from the atmospheric fields; however, for finite conductivity, ionospheric and atmospheric waves are coupled. TM modes in the atmosphere can propagate at ULF frequencies, and form global Schumann resonances, with the fundamental at 8 Hz. It has been suggested that signals that propagate at the speed of light through this atmospheric waveguide can rapidly transmit signals from the polar region to lower latitudes during storm sudden commencements.

1. Introduction

ULF waves, at approximately 1 mHz to 1 Hz, play a major role in propagating energy throughout the magnetospheric system. At the lowest end of this frequency band, the wavelength of ULF waves is comparable to the entire magnetosphere. In this frequency range, the global structure of the magnetosphere can lead to global cavity resonances and waveguide modes (see articles by *Wright and Mann, Lee and Takahashi, and Rankin et al.*, this volume). The structure of these modes is determined by the gradients in the Alfvén and fast mode speeds in the magnetospheric system.

These gradients are particularly strong in the region up to about 1 R_E altitude, since the mass density decreases exponentially with increasing altitude while the magnetic field falls off less rapidly. Thus, the Alfvén speed increases rapidly, reaching a peak at an altitude of about 1 R_E that can be comparable to the speed of light. The behavior in the wave speed for typical parameters based on the MSIS and IRI models is shown in Figure 1, with the top panel giving the wave speed up to 10,000 km, while the lower panel focuses in the lowest 1000 km of the field line. The deep minimum in the wave speed in the ionosphere forms a resonant cavity, termed the ionospheric Alfvén resonator by *Polyakov and Rapaport* (1981) and studied extensively by *Trakhtengertz and Feldstein* (1984, 1991) and *Lysak* (1986, 1988, 1991, 1993). This cavity has resonant frequencies in the range of 0.1-1.0 Hz.

It has long been known from ground observations that Pc1 waves in this band are common in the ionosphere (e.g., *Jacobs and Watanabe*, 1962; *Manchester*, 1968; *Fraser*, 1975; *Hansen et al.*, 1992; *Popecki et al.*, 1993; *Neudegg et al.*, 1995). Simultaneous observations of Pc1 waves by ground magnetometers and the Viking satellite have been reported by *Arnoldy et al.* (1988, 1996) and *Potemra et al.* (1992). Less structured waves in this band are the PiB bursts observed in the midnight sector associated with substorms (e.g., *Heacock*, 1967; *Bösinger et al.*, 1981; *Koskinen et al.*, 1993). These PiB bursts are typically associated with the arrival of the substorm current wedge at the ionosphere, and may be associated with conductivity enhancements due to localized precipitation (*Grant and Burns*, 1995).

Waves in this frequency range have frequently been observed by satellites and sounding rockets. *Temerin et al.* (1981) noted that S3-3 satellite observations of large quasi-static electric fields are consistent with being electrostatic structures at high altitudes; at altitudes below 5000 km; however, the observed electric fields were more consistent with being large amplitude Alfvén waves. Dynamics Explorer observations (*Gurnett et al.*, 1984) have also indicated that low frequency electric and magnetic field observations are consistent with an Alfvén wave interpretation. Similar results have been obtained by the ICB-1300 satellite (*Chmyrev et al.*, 1985), Aureol-3 (*Berthelier et al.*, 1989), Magsat (*Iyemori and Hayashi*, 1989), HILAT (*Knudsen et al.*, 1990, 1992), Freja (*Grzesiak*, 2000), FAST (*Chaston et al.*, 2002b), Akebono (*Hirano et al.*, 2005) and sounding rockets (*Boehm et al.*, 1990). Viking observations have shown that the peak power of electric and magnetic fluctuations occurs in this same frequency range (*Marklund et al.*, 1990; *Block and Fälthammar*, 1990; *Erlandson et al.*, 1990). It is interesting to note that *Volwerk et al.* (1996) report a small compressional component in association with the Alfvén wave, consistent with a coupling between these two wave modes. *Arnoldy et al.* (1998) observed Pi1 waves simultaneously at the GOES spacecraft and on the ground. These observations indicated that although the general frequency response at the satellites and the ground were similar, there were significant differences both in the spectral width of the emissions and in the timing of the event, indicating that the wave signature was modified by wave propagation through the ionosphere.

While the density structure above the ionosphere leads to a resonance cavity for shear Alfvén waves, it provides a waveguide for compressional waves that can propagate across field lines (e.g., *Greifinger and Greifinger*, 1968). Therefore, a signal observed on the ground may not be on the same field line as the field-aligned current structure that produced it. *Neudegg et al.* (1995) have shown from an array of ground magnetometers that Pc1 signals propagate with a typical speed of 450 km/s over distances of a few hundred kilometers, consistent with propagation in this ionospheric waveguide. *Yahnina et al.* (2000) have noted that Pc1 oscillations can be seen a few hours of magnetic local time away from their source. These observations indicate that these waves can propagate over large distances through the ionosphere. Over such long distances, the magnetic field dip angle will change and so models that assume a vertical field will have to be modified. The early work of *Greifinger and Greifinger* (1968, 1973) indicates that waves polarized in the poloidal or toroidal directions will interact with the ionosphere differently due to dip angle effects. *Fujita and Tamao* (1988) studied the propagation of Pc1 waves in a simplified model, and also found changes in the polarization as the wave propagated.

The shear waves trapped in the ionospheric Alfvén resonator and the compressional waves propagating in the waveguide can be coupled by means of Hall currents in the ionosphere. *Yoshikawa and Itonaga* (1996, 2000) have recently analyzed this coupling and noted that the

reflection characteristics of Alfvén waves from the ionosphere is modified by including inductive (i.e., non-electrostatic) effects at the ionospheric boundary. This work has noted that the electrostatic ionospheric boundary condition often used in descriptions of magnetosphere-ionosphere coupling must be modified to take into account the inductive effects.

In addition, electromagnetic waves can also propagate through the atmosphere in a waveguide bounded by the conducting ionosphere and the ground. These modes can be classified as TE (transverse electric) or TM (transverse magnetic), for which the component of the electric or magnetic field (respectively) in the direction of propagation vanishes. It can be shown (see below) that the TE modes have a minimum frequency that is the order of the speed of light divided by the ionospheric height, or about 3 kHz, and thus fall out of the ULF range. However, the TM mode can in principle have much lower frequencies. The most prominent features in the spectrum of these modes are the Schumann resonances (*Schumann, 1952*), with the fundamental frequency at about 8 Hz. These resonances can be excited by any electromagnetic disturbance in the atmosphere, most notably by lightning strikes. Moreover, *Kikuchi and Araki (1979a,b)* have proposed that waves at even lower frequencies can propagate in this mode. They suggest that this propagation may be responsible for the rapid transmission of perturbations from storm sudden commencements over the entire globe.

Although these ionospheric and atmospheric modes can be treated separately in the limit of infinite ionospheric conductivity, they are coupled in the general case of finite conductivity. Indeed, this coupling is responsible for the fact that magnetic perturbations of magnetospheric origin can be observed from the ground at all. This coupling has recently been invoked by *Surkov et al. (2005)*, who suggested that thunderstorms could excite modes of the ionospheric Alfvén resonator.

The purpose of this paper is to review the theory of these various resonant cavities and waveguides and their couplings. The following section will discuss the ionospheric Alfvén resonator, treating it in isolation from the other modes. We will treat the ionospheric waveguide in a similar manner in section 3, while section 4 will discuss the role of the Hall conductivity in coupling these modes. We will consider the modes in the atmosphere in section 5 and their coupling to the magnetospheric waves in section 6. This will be followed by some general conclusions.

2. Theory of the Ionospheric Alfvén Resonator

In order to understand these various cavities and waveguides, we will adopt the simplest possible model that contains the important features of the problem. First of all, we will consider a cold plasma with straight, vertical magnetic field lines. We will assume ideal MHD, so that the parallel electric field is set to zero. These assumptions are reasonable, particularly for high latitudes, since the magnetic zenith angle is small at the poles, and the magnetic field is so strong that plasma pressure effects can be ignored (in other words, the β of the plasma is very low, which is generally true in the ionosphere and low-altitude magnetosphere). We are interested here in fields with large perpendicular scale, and for such fields the effects of parallel electric fields can be ignored (e.g., *Lysak and Song, 2001*). The model used is based on the linearized MHD equations, which can be conveniently written in terms of Maxwell's equations:

$$\frac{\partial \mathbf{B}}{\partial t} = -\nabla \times \mathbf{E} \quad (1)$$

$$\varepsilon_{\perp} \frac{\partial \mathbf{E}_{\perp}}{\partial t} = \frac{1}{\mu_0} (\nabla \times \mathbf{B})_{\perp} \quad (2)$$

where $\varepsilon_{\perp} = \varepsilon_0(1 + c^2/V_A^2)$ is the low-frequency dielectric constant for a plasma. Note that in the ionosphere and much of the magnetosphere, the Alfvén speed is much less than the speed of light; however, it can approach c in the auroral acceleration region as well as in the neutral atmosphere and so in this case the displacement current term must be included. Effects of relaxing these assumptions will be discussed at the end of the section.

If we consider a plane wave variation in the perpendicular direction $\exp(ik_{\perp}x)$ and consider oscillations at a frequency ω , an ideal shear mode Alfvén wave will consist of E_x and b_y components, where z is the vertical direction, parallel or anti-parallel to the magnetic field in the southern and northern ionospheres, respectively. Here we use a lower case b for the perturbation field in order to distinguish it from the background field. In this case, equations (1) and (2) can be combined into a wave equation

$$\frac{\partial^2 E_x}{\partial z^2} + \frac{\omega^2}{V_A^2(z)} E_x = 0 \quad (3)$$

The next step is to choose a profile for the Alfvén speed along the field line. Some authors (e.g., *Trakhtengertz and Feldstein*, 1984; *Fedorov et al.*, 2001; *Pilipenko et al.*, 2002; *Surkov et al.*, 2005) have used a step-wise Alfvén speed profile, but it is more realistic and not much more difficult to introduce a modified exponential profile, as suggested by *Greifinger and Greifinger* (1968), and used extensively in models of the ionospheric Alfvén resonator (e.g., *Polyakov and Rapoport*, 1981; *Trakhtengertz and Feldstein*, 1991; *Lysak*, 1991, 1999; *Pokhotelov et al.*, 2000; *Grzesiak*, 2000):

$$V_A^2(z) = \frac{V_{AI}^2}{\varepsilon^2 + e^{-z/h}} \quad (4)$$

Notice that for this profile, the Alfvén speed approaches $V_{AM} = V_{AI} / \varepsilon$ as $z \rightarrow \infty$, and V_{AI} is the Alfvén speed at the ionosphere for $\varepsilon \ll 1$. Note that while this profile accurately models the increase of the Alfvén speed above the ionosphere, it assumes that the Alfvén speed becomes constant at high altitude rather than the slow decrease above the Alfvén speed peak seen in Figure 1. It was noted by *Lysak* (1993) that use of a more realistic profile does not change mode structure qualitatively. Inserting the profile (4) into the wave equation (3) gives

$$\frac{\partial^2 E_x}{\partial z^2} + \frac{\omega^2}{V_{AI}^2} (\varepsilon^2 + e^{-z/h}) E_x = 0 \quad (5)$$

Although this equation looks complicated, it can be simplified by a substitution $x = x_0 e^{-z/2h}$, where $x_0 = 2h\omega/V_{AI}$, in which case it turns into a form of Bessel's equation

$$x^2 \frac{\partial^2 E_x}{\partial x^2} + x \frac{\partial E_x}{\partial x} + (\varepsilon^2 x_0^2 + x^2) E_x = 0 \quad (6)$$

which has solutions that are Bessel functions of order $\nu^2 = -x_0^2 \varepsilon^2$:

$$E_x = E_1 J_{ix_0 \varepsilon}(x) + E_2 J_{-ix_0 \varepsilon}(x) \quad (7)$$

Note that in these solutions, $x = x_0$ is the ionosphere and $x = 0$ is the magnetosphere. Note that for small values of x , the Taylor expansion of the Bessel function gives the approximation

$$J_{\pm ix_0 \varepsilon}(x) \approx \frac{(x/2)^{\pm ix_0 \varepsilon}}{\Gamma(1 \pm ix_0 \varepsilon)} = \frac{(x_0/2)^{\pm ix_0 \varepsilon}}{\Gamma(1 \pm ix_0 \varepsilon)} e^{\mp i\omega z/V_{AM}} \quad (8)$$

This solution indicates that the solutions become plane waves propagating in the $\mp z$ direction. Since we are concerned with solutions that do not require the input of energy from above, we will take the $-$ solution in what follows.

To find the normal modes of this resonator, we must apply an ionospheric boundary condition. For the time being, we will neglect the Hall conductance and consider a slab model for the ionosphere, characterized by a Pedersen conductance Σ_P . Assuming no field perturbations or currents exist below the ionosphere, the electromagnetic jump condition over the ionospheric slab can be written as

$$\mu_0 \Sigma_P \mathbf{E} = \hat{\mathbf{z}} \times \mathbf{b} \quad \Rightarrow \quad \mu_0 \Sigma_P E_x + b_y = 0 \quad (9)$$

where the last form applies in the current situation. Here we have introduced the lower case \mathbf{b} to denote the magnetic perturbation. Noting from equation (1) that $b_y = -(i/\omega)\partial E_x/\partial z$, we find that the boundary condition can be written as

$$\frac{\partial E_x}{\partial z} + i\omega\mu_0\Sigma_P E_x = 0 \quad (\text{at } z = 0) \quad (10)$$

Transforming to the variable x and defining $\alpha_P = \mu_0 V_{AM} \Sigma_P$, equation (10) can be written as

$$\frac{x}{x_0} \frac{\partial E_x}{\partial x} - i\alpha_P E_x = 0 \quad (11)$$

At the ionosphere, $x = x_0$, and so the dispersion relation takes the form (e.g., *Lysak*, 1991).

$$J'_{-ix_0 \varepsilon}(x_0) - i\alpha_P J_{-ix_0 \varepsilon}(x_0) = 0 \quad (12)$$

This dispersion relation can be solved numerically for x_0 . The solutions can be seen approximately in the limit $x_0 \varepsilon \ll 1$, which is typically the case. In this limit, the Bessel function can be written as

$$J_{-ix_0 \varepsilon}(x) = J_0(x) - ix_0 \varepsilon \frac{\pi}{2} Y_0(x) \quad (13)$$

In this case, the solution for a poor conductor, $\alpha_P \ll 1$, is given by the zeroes of the derivative of J_0 , which is equal to $-J_1$. Thus the first three roots are given by $x_0 = 3.83, 7.02, 10.17$. The growth rate γ can be given by expanding equation (13) to first order in α_P and ε , resulting in

$$\gamma = \frac{V_{AM}}{2h} \varepsilon \frac{\pi}{2} \frac{\xi Y_1(\xi)}{J_0(\xi)} \quad (14)$$

where ξ is a zero of J_1 . The Bessel functions satisfy the Wronskian condition

$$J_1(x)Y_0(x) - J_0(x)Y_1(x) = \frac{2}{\pi x} \quad (15)$$

Therefore, Y_1 and J_0 always have opposite sign when $J_1 = 0$, so the growth rate is always negative, indicating damping.

On the other hand, in the good conductivity limit, $\alpha_P \rightarrow \infty$, the solutions are the zeroes of J_0 , with the first three being 2.40, 5.52 and 8.65. (Note that for a more realistic profile such as in Figure 1, *Lysak* (1993) showed that these coefficients were reduced to 2.1, 4.8 and 7.4.) In this case the growth rate can be found by expanding in $1/\alpha_P$ and ε , yielding

$$\gamma = \frac{V_{Al}}{2h} \left[-\frac{1}{\alpha_p} - \frac{\varepsilon\pi}{2} \frac{\xi Y_0(\xi)}{J_1(\xi)} \right] \quad (16)$$

where now ξ is a zero of J_0 . Equation (15) indicates that Y_0 and J_1 always have the same sign when $J_0 = 0$; thus, both terms of equation (16) contribute damping. Note that corresponding results for the stepwise Alfvén speed profile are discussed in the Appendix.

It should be noted that for a typical Alfvén speed at the ionosphere of 1000 km/s range (corresponding to a density of $3.0 \times 10^5 \text{ cm}^{-3}$ if O^+ is the dominant ion), and the scale height of the ionosphere is the order of 500 km. Thus, for these parameters the base angular frequency of $V_{Al}/2h$ is 1.0 s^{-1} or a frequency of 0.16 Hz. Thus the fundamental eigenmode of the ionospheric resonator is 0.38 to 0.61 Hz for the good conductivity and poor conductivity cases, respectively.

Recent observations have verified that waves in this frequency range are common, not only at auroral latitudes but also at lower latitudes. *Belyaev et al.* (1999) have observed the spectral signatures of the resonator from ground magnetometer observations, and have shown that the frequency structure was consistent with the resonator, and varied during the day consistent with ionospheric density measurements from the EISCAT radar. *Grzesiak* (2000) showed using Freja data that the phase relationships predicted by the theory of the resonator (*Lysak*, 1991) were consistent with the data. Recent observations from Akebono (*Hirano et al.*, 2005) and from a sounding rocket (*Tanaka et al.*, 2005) have shown IAR signatures in the cusp and the related modulation of precipitating electrons.

New theoretical developments beyond the basic theory presented above have concentrated on the interaction of the resonator with parallel electric fields and the acceleration of auroral particles. *Lysak* (1993) included electron inertia and a more realistic Alfvén speed profile based on a dipole magnetic field to show that effects from the resonator persisted when parallel electric fields were present. This model was used to investigate electron acceleration through test particle models (*Thompson and Lysak*, 1996; *Chaston et al.*, 2000, 2002a), indicating that field-aligned beams of electrons as observed from the FAST satellite were consistent with acceleration due to parallel electric fields in the resonator. The role of parallel electric fields at strengthening the reflection of Alfvén waves near the Alfvén speed peak has been emphasized by *Pilipenko et al.* (2002, 2004). Although these authors consider the reflection from the parallel electric field region as defining a different resonator, the same low densities that produce the Alfvén speed peak also favor the formation of parallel electric fields, thus it seems that parallel electric fields really modify the ionospheric Alfvén resonator rather than represent a new resonator.

Another role of the ionospheric Alfvén resonator is to modify the ionospheric feedback instability (e.g., *Atkinson*, 1970; *Sato*, 1978; *Lysak*, 1991). This instability can be caused when the ionospheric conductivity changes produced by electron precipitation modify the field-aligned current system. When the newly produced currents reinforce the conductivity changes, a strong structuring of both can occur. Simulations of the feedback instability (*Pokhotelov et al.*, 2002a,b; *Lysak and Song*, 2002) show that this instability, which was originally formulated based on the field line resonance, operates much more quickly when coupled to the ionospheric resonator. The structuring of auroral currents produced by this instability operates more readily in a low-conductivity ionosphere (*Pokhotelov et al.*, 2002b), possibly explaining observations showing that discrete electron precipitation occurs primarily in the dark ionosphere (*Newell et al.*, 1996).

3. Theory of the Ionospheric Waveguide

A similar description as that given in section 2 can be developed for the compressional mode in the ionospheric waveguide. If, as before, we assume a vertical background magnetic field in the z direction and a wave vector in the x direction, the fast mode consists of the E_y , b_x , and b_z components. Applying Faraday's Law, equation (1), we can relate the magnetic components to the electric field as

$$b_x = \frac{i}{\omega} \frac{\partial E_y}{\partial z} \quad b_z = \frac{k_\perp}{\omega} E_y \quad (17)$$

These relations can be inserted into Ampere's Law, equation (2) to find

$$\frac{\partial^2 E_y}{\partial z^2} + \left(\frac{\omega^2}{V_A^2(z)} - k_\perp^2 \right) E_y = 0 \quad (18)$$

Note that the only difference from equation (3) is the presence of k_\perp , which enters since this mode can propagate perpendicular to the magnetic field. If the exponential Alfvén speed profile given by equation (4) is used, then equation (18) becomes

$$\frac{\partial^2 E_y}{\partial z^2} + \left(\frac{\omega^2}{V_{Al}^2} (\epsilon^2 + e^{-z/h}) - k_\perp^2 \right) E_y = 0 \quad (19)$$

If we now use the same substitution as above, $x = x_0 e^{-z/2h}$, then equation (19) can be written in terms of Bessel's equation

$$x^2 \frac{\partial^2 E_y}{\partial x^2} + x \frac{\partial E_y}{\partial x} - (4k_\perp^2 h^2 - x_0^2 \epsilon^2 - x^2) E_y = 0 \quad (20)$$

This equation can be written in terms of Bessel functions of order $\nu = \sqrt{4k_\perp^2 h^2 - x_0^2 \epsilon^2}$

$$E_y = AJ_\nu(x) + BJ_{-\nu}(x) \quad (21)$$

Note that for this case there are two possible outcomes: (1) if $2k_\perp h > x_0 \epsilon$, or in other words, if $k_\perp > \omega/V_{AM}$, the order ν is real and the positive solution should be chosen so that the solution is finite at $x = 0$ (recall that this corresponds to $z \rightarrow \infty$); (2) if $2k_\perp h < x_0 \epsilon$, the order is purely imaginary and the negative solution corresponds to upward propagating waves, as in the shear mode case (see equation (8)). Both cases can be included if we write the solution as

$$E_y = E_0 J_\nu(x) \quad (\text{Re } \nu \geq 0; \text{Im } \nu \leq 0) \quad (22)$$

Next, as before, we should apply the appropriate boundary conditions at the ionosphere. We can use the jump conditions over the ionospheric slab as in equation (9); however, in this case, we cannot in general assume that the fields below the ionosphere are equal to zero. In this case we should write

$$\hat{\mathbf{z}} \times [\mathbf{b}] = \mu_0 \Sigma_p \mathbf{E} \quad \Rightarrow \quad b_x^{mag} - b_x^{atm} = \mu_0 \Sigma_p E_y \quad (23)$$

Note that in addition the tangential component of \mathbf{E} must be continuous across this boundary. Here b_x^{mag} and b_x^{atm} represent the magnetic perturbations just above (magnetosphere) and just below (atmosphere) the ionosphere, respectively. The magnetospheric magnetic field can be written using equation (17), which translated into the variable x becomes

$$b_x^{mag} = \frac{i}{V_{Al}} \frac{x}{x_0} E_0 J'_\nu(x) \quad (24)$$

Unlike in the shear mode case, we must consider the perturbations in the atmosphere for this mode. Indeed, it is mainly the contribution from this mode that gives rise to the magnetic signal seen on the ground. The simplest possible model for the atmosphere is a perfectly insulating slab, terminated by the perfectly conducting ground (a more complete model will be discussed in section 6). In this case, the permittivity in equation (2) is simply ϵ_0 , and so waves propagate at the speed of light. In this case the wave equation (18) is replaced by

$$\frac{\partial^2 E_y}{\partial z^2} + \left(\frac{\omega^2}{c^2} - k_{\perp}^2 \right) E_y = 0 \quad (25)$$

Note that in this expression $c/\omega = 47,000$ km for $\omega/2\pi = 1$ Hz, greater than the circumference of the Earth. In this case, the solutions are upgoing and downgoing attenuated waves

$$E_y = E_1 e^{\kappa_a z} + E_2 e^{-\kappa_a z} \quad (26)$$

where $\kappa_a = \sqrt{k_{\perp}^2 - \omega^2/c^2}$, and the subscript a indicates the atmosphere. For wavelengths much less than c/ω , $\kappa_a \approx k_{\perp}$. Using equation (17), we can then write the magnetic perturbation as

$$b_x^{atm} = \frac{i\kappa_a}{\omega} (E_1 e^{\kappa_a z} - E_2 e^{-\kappa_a z}) \quad (27)$$

If we let the ionosphere be at $z = 0$, the surface of the Earth will be at $z = -d$, where $d \sim 80$ km is the thickness of the atmosphere. For a perfectly conducting Earth, the electric field must vanish at $z = -d$, and so equations (26) and (27) can be written as

$$E_y^{atm} = E_a \sinh \kappa_a (z + d) \quad b_x^{atm} = \frac{i\kappa_a}{\omega} E_a \cosh \kappa_a (z + d) \quad (28)$$

Now we can apply the boundary conditions (23) at the ionosphere, $z = 0$:

$$E_a \sinh \kappa_a d = E_0 J_v(x_0) \quad (29)$$

$$-\frac{i}{V_{AI}} E_0 J'_v(x_0) - \frac{i\kappa_a}{\omega} E_a \cosh \kappa_a d = \mu_0 \Sigma_P E_0 J_v(x_0)$$

Combining these relations gives the dispersion relation for the fast mode

$$J'_v(x_0) - \left[i\alpha_P + \frac{\kappa_a V_{AI}}{\omega} \coth \kappa_a d \right] J_v(x_0) = 0 \quad (30)$$

where $\alpha_P = \mu_0 V_{AI} \Sigma_P$ as before. For typical parameters, the atmospheric correction term is of order unity, and so cannot be neglected except in the high conductivity case, $\alpha_P \rightarrow \infty$. Numerical solutions of this equation are shown in Figures 2 and 3. This figure shows the wave frequency, polarization (defined as E_a/E_0) and the perpendicular group velocity of these waves. This plot assumes $V_{AI} = 1000$ km/s, $\epsilon = 0.01$, $h = 1000$ km, $d = 80$ km and $\Sigma_P = 10.0$ mho (Figure 2) and 0.1 mho (Figure 3). In the high conductivity case, there is very little electric field in the atmosphere, as indicated by the low polarization values. For large α_P , the first term in the brackets of equation (30) is dominant and the dispersion relation is basically $J_v(x_0) = 0$. As $k_{\perp} \rightarrow 0$, the solutions then become the zeroes of J_0 . Note that the group velocity in this case is about 1.5 times the ionospheric Alfvén speed. On the other hand, for low conductivity, the two terms in the brackets are both small as $k_{\perp} \rightarrow 0$, and the solutions become approximately $J'_v(x_0) = 0$, going to roots of $J'_0 = -J_1$ for small k_{\perp} . Note that the zero root, which did not enter in the case of the ionospheric resonator, is present in this case and has finite frequency for finite k_{\perp} . In this case, there is a more significant coupling to the atmospheric wave.

The propagation of signals in the Pc1 range through the ionospheric waveguide is well documented. Multi-station observations of Pc1 waves by *Fraser (1975)* and *Althouse and Davis (1978)* showed that the waves propagated at speeds in the range 500-2000 km/s, consistent with the model presented above. More recently, *Neudegg et al., (1995)* used an array of ground magnetometers to show that high-latitude Pc1 signals propagated at speeds of 450 km/s over distances of up to 1000 km. *Yahnina et al. (2000)* have noted that Pc1 oscillations can be seen a few hours of magnetic local time away from their source. A numerical model of ULF wave propagation in a dipole magnetosphere (*Lysak, 2004; Lysak and Song, 2005*) has shown that signals in this frequency range can readily propagate world-wide over periods of tens of seconds. This model also serves to verify that the Pc1 waveguide is still operative at high and mid-latitudes even when dip angle effects are taken into account.

4. Hall currents and the inductive ionosphere

The preceding two sections have considered the ionospheric Alfvén resonator for shear mode waves and the ionospheric waveguide for compressional waves as separate entities, neglecting the effects of the Hall current. However, it has long been recognized that the Hall conductance is necessary to produce the signatures of ULF waves as seen on the ground (e.g., *Hughes, 1974*). Recently, *Yoshikawa and co-workers (Yoshikawa and Itonaga, 1996, 2000; Yoshikawa et al., 1999, 2002; Yoshikawa, 2002)* have emphasized the role of the Hall conductivity in coupling the wave modes in the ionosphere. This section will summarize this coupling process.

The Hall effect can be included by introducing the Hall current into equation (23):

$$\hat{\mathbf{z}} \times [\mathbf{b}] = \mu_0 \left(\Sigma_p \mathbf{E}_\perp - \Sigma_H \mathbf{E} \times \hat{\mathbf{B}} \right) \quad (31)$$

where the brackets denote the jump across the ionospheric layer as above. Note here that we distinguish between the upward vertical unit vector $\hat{\mathbf{z}}$ and the unit vector in the direction of the background magnetic field $\hat{\mathbf{B}}$. These two unit vectors are in the same direction at the south pole and opposite directions at the north pole, varying with the inclination angle of the magnetic field. For simplicity, in the following we will assume southern hemisphere conditions and set $\hat{\mathbf{B}} = \hat{\mathbf{z}}$. It should be noted that equation (31) is more general than the ionospheric boundary condition based on current continuity used in many numerical models (*Lysak and Song, 2005*). This can be seen by first taking the divergence of equation (31), assuming that the conductances are constant

$$\nabla \cdot (\hat{\mathbf{z}} \times [\mathbf{b}]) = -\hat{\mathbf{z}} \cdot (\nabla \times \mathbf{b}) = -j_z = \mu_0 \left(\Sigma_p \nabla \cdot \mathbf{E}_\perp - \Sigma_H \hat{\mathbf{z}} \cdot (\nabla \times \mathbf{E}) \right) \quad (32)$$

Note here we have assumed that the atmosphere is a perfect insulator so that there are no currents below the ionosphere. However, the condition (31) also includes a condition on the compressional magnetic field, as can be found from taking the vertical curl of equation (31) and using $\nabla \cdot \mathbf{b} = 0$:

$$\left[\frac{\partial b_z}{\partial z} \right] = \mu_0 \left(\Sigma_p \hat{\mathbf{z}} \cdot (\nabla \times \mathbf{E}) + \Sigma_H \nabla \cdot \mathbf{E}_\perp \right) \quad (33)$$

Note that while the jump in b_z is zero due to the divergence-free condition, the jump in its derivative can be non-zero. Recalling that the shear mode is characterized by a non-zero divergence of \mathbf{E}_\perp and the compressional mode by a non-zero curl of \mathbf{E}_\perp , equations (32) and (33) indicate the role that the Hall conductance plays in coupling these two modes.

This model has been used by *Yoshikawa and Itonaga* (1996) to calculate the reflection and mode conversion coefficients at the ionosphere. If it is assumed that the Alfvén speed remains constant above the ionosphere for simplicity, the equations for the shear and fast modes, respectively, can be written as

$$\begin{aligned}\nabla \cdot \mathbf{E}_\perp &= \alpha^i e^{i\omega\mu_0\Sigma_A z} + \alpha^r e^{-i\omega\mu_0\Sigma_A z} \\ \hat{\mathbf{z}} \cdot (\nabla \times \mathbf{E}) &= \beta^i e^{i\omega\mu_0\Sigma_F z} + \beta^r e^{-i\omega\mu_0\Sigma_F z}\end{aligned}\quad (34)$$

where the Alfvén conductance is $\Sigma_A = 1/\mu_0 V_A$ and the fast mode conductance is

$$\Sigma_F = -i\Sigma_A \sqrt{\left(\frac{k_\perp V_A}{\omega}\right)^2 - 1}\quad (35)$$

Note that the sign in equation (35) is chosen for a fast mode wave evanescent in the magnetosphere, $k_\perp V_A > \omega$. Furthermore, as noted in the previous section, we should include the wave transmitted into the ionosphere

$$\hat{\mathbf{z}} \cdot (\nabla \times \mathbf{E})^{atm} = \gamma \frac{\sinh[i\omega\mu_0\Sigma_{atm}(z+d)]}{\sinh[i\omega\mu_0\Sigma_{atm}d]}\quad (36)$$

where we can write

$$\Sigma_{atm} = \frac{\sqrt{(\omega/c)^2 - k_\perp^2}}{\mu_0\omega} \approx i \frac{k_\perp}{\mu_0\omega}\quad (37)$$

where the last form holds in the typical limit, $k_\perp \gg \omega/c$. Matching the boundary conditions across the ionospheric slab allows one to calculate the reflection matrix

$$\begin{pmatrix} \alpha^r \\ \beta^r \end{pmatrix} = \begin{pmatrix} R_{AA} & R_{FA} \\ R_{AF} & R_{FF} \end{pmatrix} \begin{pmatrix} \alpha^i \\ \beta^i \end{pmatrix}\quad (38)$$

where we have

$$R_{AA} = \frac{\Sigma_A - \Sigma_P - \Sigma_{AF}}{\Sigma_A + \Sigma_P + \Sigma_{AF}} \quad R_{FF} = \frac{\Sigma_F - \Sigma_P - \Sigma_{FA}}{\Sigma_F + \Sigma_P + \Sigma_{FA}}\quad (39)$$

In these expressions, the additional terms represent the mode coupling:

$$\Sigma_{AF} = \frac{\Sigma_H^2}{\Sigma_P - \Sigma_F - \Sigma_{atm} \coth k_\perp d}\quad (40)$$

$$\Sigma_{FA} = \Sigma_{atm} \coth k_\perp d - \frac{\Sigma_H^2}{\Sigma_A + \Sigma_P}\quad (41)$$

The off-diagonal terms in this expression, representing the coupling of the fast and shear Alfvén branches, can then be written as

$$R_{AF} = (1 + R_{AA}) \frac{\Sigma_{AF}}{\Sigma_H} \quad R_{FA} = (1 + R_{FF}) \frac{\Sigma_{FA}}{\Sigma_A + \Sigma_P}\quad (42)$$

It should be noted that the additional terms associated with the mode coupling become more important for large scale (small k_\perp) and high frequency perturbations. This follows since both Σ_F and Σ_{atm} are large for small k_\perp/ω , and so the coupling terms represented by Σ_{AF} and Σ_{FA} become small in this limit. The condition for the importance of the inductive coupling term can roughly be written as $\omega/k_\perp \gg 1/\mu_0\Sigma_{crit}$, where Σ_{crit} is the smaller of Σ_P and Σ_H^2/Σ_p . Note that

the right-hand side of this expression is 800 km/s for $\Sigma_{crit} = 1$ mho. These considerations suggest that the mode coupling is most efficient for Pc1 waves that have large perpendicular scales, which are the waves that can be seen on the ground. This point was emphasized by *Pokhotelov et al.* (2000) who analyzed the ionospheric feedback instability with an inductive ionosphere. Since the feedback instability tends to produce small perpendicular scales, the mode coupling is a small effect on feedback models. On the other hand, *Yoshikawa et al.* (1999) have shown that inductive effects also can modify the mode structure and damping of field-line resonances, even when they are not dominant. In particular, these effects can resolve the singularity that occurs at the resonance.

At this point, it would be useful to examine the limitations of the height-integrated ionosphere assumption. Treating the ionosphere as a thin slab requires that the electromagnetic fields can indeed penetrate through the entire ionospheric layer. To assess this effect, note that in an isotropic conductor, basic electromagnetic theory (e.g., *Jackson*, 1999) shows that a wave will be evanescent with a scale length given by the collisional skin depth, $\delta_p = \sqrt{2/\omega\mu_0\sigma_p}$. At a frequency of $\omega/2\pi = 1$ Hz and a conductivity of 10^{-4} mho/m, a typical value of the ionospheric Pedersen conductivity, this skin depth is 50 km, comparable to the Pedersen current-carrying region of the ionosphere. Thus, while the thickness of the ionosphere is negligible for very low frequency waves such as field line resonances, this may not be applicable for waves in the Pc1 range.

Another limiting effect comes as a result of the parallel conductivity of the ionosphere. While this conductivity is very large in the magnetosphere, it is reduced to values of the order of 1 mho/m in the E-layer of the ionosphere (e.g., *Kelley*, 1989). At this point there is a skin depth associated with this conductivity that can be written as $\delta_{\parallel} = (1/k_{\perp})\sqrt{\sigma_{\parallel}/\sigma_p}$. For a perpendicular wavelength of 100 km, this scale length is quite large, ~ 1600 km. However, for small perpendicular wavelengths ~ 1 km such as might be associated with auroral arcs, this effect can be significant. However, for waves that will propagate in the ionospheric waveguide and be seen on the ground, this effect is not important.

Note that a complete theory of the thick ionosphere requires the consideration of both fast and Alfvén modes, which are coupled by the Hall conductivity. By writing Faraday's and Ampere's Law with an assumed $\exp(ik_{\perp}x - i\omega t)$ dependence, we find

$$\begin{aligned}
-i\omega b_x &= \frac{\partial E_y}{\partial z} & -\frac{i\omega}{V^2} E_x &= -\frac{\partial b_y}{\partial z} + \mu_0\sigma_p E_x - \mu_0\sigma_H E_y \\
-i\omega b_y &= -\frac{\partial E_x}{\partial z} + ik_{\perp} E_z & -\frac{i\omega}{V^2} E_y &= \frac{\partial b_x}{\partial z} - ik_b z + \mu_0\sigma_p E_y + \mu_0\sigma_H E_x \\
-i\omega b_z &= -ik_{\perp} E_y & -\frac{i\omega}{c^2} E_z &= ik_b y + \mu_0\sigma_{\parallel} E_z
\end{aligned} \tag{43}$$

These equations illustrate that in the absence of Hall conductivity, b_x , b_z , and E_y give the fast mode and E_x , E_z , and b_y give the shear Alfvén mode. If we assume that the conductivities and the wave velocity V (which is the Alfvén speed at higher altitudes but becomes the speed of light in the lower E-layer) are constant in a slab, we can rewrite these equations as

$$\frac{\partial^2 b_x}{\partial z^2} = \left(k_{\perp}^2 - \frac{\omega^2}{V^2} + i\omega\mu_0\sigma_p \right) b_x - \mu_0\sigma_H \left(i\omega + \frac{k_{\perp}^2}{\mu_0\sigma_{\parallel}} \right) b_y \tag{44}$$

and

$$\frac{\partial^2 b_y}{\partial z^2} = \left(k_{\perp}^2 \frac{\sigma_p}{\sigma_{\parallel}} - \frac{\omega^2}{V^2} + i\omega \left(\mu_0 \sigma_p + \frac{k_{\perp}^2}{\mu_0 \sigma_{\parallel} V^2} \right) \right) b_y + i\omega \mu_0 \sigma_H b_x \quad (45)$$

Note that the classical skin depth formulas follow from neglecting the terms with V^2 in the denominator, which is justified when the velocity becomes c , but may not be when it is the Alfvén speed. Setting the spatial derivative $\partial/\partial z \rightarrow \kappa$ and dropping the parallel conductivity terms, one can find the general expressions for the scale lengths

$$\kappa^2 = \frac{k_{\perp}^2}{2} - \frac{\omega^2}{V^2} + i\omega \mu_0 \sigma_p \pm \frac{1}{2} \sqrt{k_{\perp}^4 + 4\omega^2 \mu_0^2 \sigma_H^2} \quad (46)$$

where the top sign is the fast mode and the bottom is the Alfvén mode for zero Hall conductivity. Note that the effective skin depth in each case is given by the positive real part of κ .

The important point is that for high conductivity and high frequency, the finite skin depth will shield the magnetospheric and atmospheric fields from one another. However, under less extreme conditions, the fields can penetrate and these fields are coupled. Analysis of this coupled magnetosphere-ionosphere-atmosphere system will be discussed in the next sections.

5. Atmospheric Waveguide Modes

Electromagnetic waves can also propagate in an atmospheric waveguide bounded by the conducting ionosphere and the conducting ground. As a first approximation, the atmosphere can be considered to be a perfect insulator compared with these conducting boundaries, and then Maxwell's equations in a vacuum can be used. In the same geometry as we discussed above with the x direction assumed to be the direction of horizontal variations, the wave equations break up into TE and TM modes, with the TE mode containing b_x , b_z , and E_y and the TM mode containing E_x , E_z , and b_y . By comparison with the description above it is clear that the TE mode corresponds to the fast MHD mode and the TM mode to the shear Alfvén mode in the plasma. The basic wave equations then are the following:

$$\begin{aligned} -i\omega b_x &= \frac{\partial E_y}{\partial z} & -\frac{i\omega}{c^2} E_x &= -\frac{\partial b_y}{\partial z} \\ -i\omega b_z &= -ik_{\perp} E_y & -\frac{i\omega}{c^2} E_z &= ik_{\perp} b_y \\ -\frac{i\omega}{c^2} E_y &= \frac{\partial b_x}{\partial z} - ik_{\perp} b_z & -i\omega b_y &= -\frac{\partial E_x}{\partial z} + ik_{\perp} E_z \end{aligned} \quad (47)$$

These are now arranged with the TE mode in the left column and the TM mode in the right column. Reducing these to a single wave equation leads to similar equations for both modes:

$$\frac{\partial^2 E_y}{\partial z^2} = \left(k_{\perp}^2 - \frac{\omega^2}{c^2} \right) E_y \quad \frac{\partial^2 b_y}{\partial z^2} = \left(k_{\perp}^2 - \frac{\omega^2}{c^2} \right) b_y \quad (48)$$

The solutions to these equations takes the form

$$E_y = E_1 e^{ik_A z} + E_2 e^{-ik_A z} \quad (49)$$

and similarly for b_y , where $k_A = \sqrt{\omega^2/c^2 - k_{\perp}^2}$, which could of course be imaginary.

The distinction between these two modes lies in the boundary conditions. If the ionosphere and atmosphere are both assumed to be perfect conductors, then the horizontal

electric fields must vanish at these boundaries. For the TE mode, this implies that $E_y = 0$ at those boundaries, but for the TM mode, requiring $E_x = 0$ implies that $\partial b_y / \partial z = 0$. Applying these boundary conditions to the TE mode gives the solution $E_y = E_0 \sin k_A z$, where $k_A = n\pi/d$, where d is the altitude of the ionosphere. It can be clearly seen that the $n = 0$ solution gives a null result, so the lowest possible TE mode is given by $n = 1$, which implies the dispersion relation $\omega_{TE,1} = c\sqrt{k_\perp^2 + (\pi/d)^2}$, or a lower cutoff frequency of $\pi c/d$. For a nominal ionospheric height of 100 km, this cutoff frequency is about 1.5 kHz, well above the ULF range. Thus the ULF TE mode is always evanescent. At ULF frequencies, this implies that the electromagnetic fields on the ground are smaller than those at the ionosphere by a factor of $e^{-k_\perp d}$; thus, waves with perpendicular wavelengths much less than the ionospheric height are not seen on the ground.

On the other hand, the TM mode would give the solution $b_y = b_0 \cos k_A z$, and in this case the $n = 0$ solution gives finite fields b_y and E_z , with a dispersion relation $\omega_{TM,0} = k_\perp c$, with a zero frequency cutoff and $k_A = 0$, implying that these fields are constant in z . Note that this mode might properly be called the transverse electromagnetic (TEM) mode since both the electric and magnetic fields are perpendicular to the propagation direction. The zero frequency cutoff of this mode led *Kikuchi and Araki* (1979a,b) to assert that energy could be transmitted in this mode through the atmosphere, providing a means for the rapid communication of signals such as the preliminary reverse impulse (PRI) of a storm sudden commencement globally, although this idea remains controversial (e.g., *Chi et al.*, 2001, 2002; *Kikuchi and Araki*, 2002).

While the existence of this mode in a planar waveguide filled with a perfect insulator, there are a number of issues in applying this mode to the atmosphere. First of all, the atmosphere is not planar, but rather a spherical shell. This suggests that it acts more like a resonant cavity than a waveguide. Indeed, it is well known (e.g., *Galejs*, 1972; *Jackson*, 1999) that this cavity supports the so-called Schumann resonances, with a fundamental frequency of about 8 Hz. The resonant frequencies of these modes for perfectly conducting boundaries is given by

$$\omega_l = \sqrt{l(l+1)} \frac{c}{a} \quad (50)$$

where a is the radial distance in the center of the cavity (essentially the radius of the Earth). This expression gives a fundamental frequency ($l = 1$) of about 10 Hz; the reduction to the observed 8 Hz value can be associated with the fact that the ionosphere and upper atmosphere are not perfect conductors (e.g., *Galejs*, 1972, Table 7.1). Note that the fundamental mode roughly corresponds to a wave with a wavelength equal to the circumference of the Earth.

These considerations imply that waves in the ULF range (i.e., below the first Schumann resonance) will have wavelengths much larger than the circumference of the Earth. Under these conditions, it is difficult to think of these waves as truly being normal modes of a waveguide. Nevertheless, signals generated in this mode can propagate without being attenuated even at low frequency. For frequencies lower than the frequency of the fundamental Schumann resonance, the model of *Kikuchi and Araki* (1979a,b) can be used to determine the impulse response of the atmosphere. They have considered the response of this waveguide to a step-function impulse in time, and noted that the Laplace transform of this impulse is then proportional to $1/s$, where s is the Laplace transform parameter that can be thought of as the inverse time scale of the impulse. They found that while the TE mode is evanescent, the TM mode can propagate without very much attenuation even in the presence of ionospheric dissipation. This conclusion essentially

follows since the damping due to the finite ionospheric conductivity goes to zero when s goes to zero (i.e., at zero frequency).

Recently, *Chi et al.* (2001) have questioned whether the transmission at the speed of light in this waveguide is in fact essential for the observed timing of the PRI. Based on data from an array of ground magnetometers, they showed time differences of 10's of seconds between high and low latitude stations. They argues that such differences could be easily accounted for by wave propagation along the path proposed by *Tamao* (1964), in which a compressional wave propagates along the equator until it is mode converted to a shear Alfvén wave, which then propagates along the field line to the ionosphere. This conclusion was challenged by *Kikuchi and Araki* (2002), who argued that *Chi et al.* (2001) considered the maximum amplitude of the signal rather than the first impulse observed. Indeed, both mechanisms may thus be operating: the initial impulse may travel through the atmospheric waveguide, while most of the energy of the main signal propagates through the magnetosphere along the *Tamao* (1964) path.

6. Coupled Solutions for the wave modes

The finite conductivity of the ionosphere leads to a coupling between all of these wave modes. The first step in a fully coupled solution is to consider the coupling between the shear Alfvén mode discussed in section 2 with the atmospheric solution discussed in the previous section. If we place the ionospheric boundary at $z = 0$ and the ground at $z = -d$, the atmospheric solution for a perfectly conducting ground can be written as

$$b_y = b_a \cosh \kappa_a (z + d) \quad E_x = -\frac{ic^2}{\omega} \frac{\partial b_y}{\partial z} = \frac{-i\kappa_a c^2}{\omega} b_a \sinh \kappa_a (z + d) \quad (51)$$

Note also that in the ionospheric Alfvén resonator, we found earlier (equation (7)) that for outgoing wave solutions we could write:

$$E_x = E_0 J_{-ix_0\epsilon}(x) \quad b_y = -i\omega \frac{\partial E_x}{\partial z} = \frac{i\omega x}{2h} \frac{\partial E_x}{\partial x} = \frac{ix}{V_{AI} x_0} E_0 J'_{-ix_0\epsilon}(x) \quad (52)$$

Recall in this form that $x = x_0 e^{-z/2h}$ and $x_0 = 2h\omega/V_{AI}$. We can couple these fields by means of the boundary conditions at the ionosphere ($z = 0$ or $x = x_0$) as in equations (9) and (23), which in this case implies:

$$[E_x] = 0 \Rightarrow E_0 J_{-ix_0\epsilon}(x_0) = -\frac{i\kappa_a c^2}{\omega} b_a \sinh \kappa_a d \quad (53)$$

$$\hat{\mathbf{z}} \times [b_y] = \mu_0 \Sigma_p E_x \Rightarrow \frac{i}{V_{AI}} E_0 J'_{-ix_0\epsilon}(x_0) + \frac{i\kappa_a c^2}{\omega} b_a \sinh \kappa_a d = \mu_0 \Sigma_p E_0 J_{-ix_0\epsilon}(x_0) \quad (54)$$

Re-arranging these equations to eliminate the amplitudes gives the coupled solution

$$\left(\frac{J'_{-ix_0\epsilon}(x_0)}{J_{-ix_0\epsilon}(x_0)} - i\alpha_p \right) = \frac{\omega V_{AI}}{\kappa_a c^2} \coth \kappa_a d \quad (55)$$

where again we have used $\alpha_p = \mu_0 \Sigma_p V_{AI}$. Note that neglecting the right-hand side of this expression returns us to the expression we found in section 2, equation (12), where we neglected the atmospheric fields. Here we can see that this expression is justified, except near the point where $\kappa_a \rightarrow 0$, which is the condition for the atmospheric waveguide modes, $k_{\perp}^2 - \omega^2/c^2 = 0$.

Figure 4 shows the dispersion relation for the waveguide modes coupled to the ionosphere and magnetosphere according to equation (55). First of all, it can be seen that very long wavelengths are required for the wave modes to be in the ULF range. Secondly, note that this mode appears to be rather strongly damped. The wavy nature of the damping results from the coupling to the IAR; the resonant frequencies, which are at 0.19, 0.44, 0.69 and 0.54 Hz for this case, correspond to enhancements in the damping and a slight lowering of the ratio of atmospheric and ionospheric fields, as seen in the bottom figure. Figure 5 shows the corresponding range for the IAR modes. It can be seen that these modes are essentially at constant frequencies; however, the damping rate is reduced at the points where the IAR modes cross the atmospheric waveguide modes. This can also be seen in the enhancements of the atmospheric fields in the bottom panel. It should be realized, however, that these effects are at very long wavelengths. Waves with more typical wavelengths of a few thousand kilometers will not be affected by the presence of the atmospheric waveguide.

For comparison, note the corresponding equation for the fast/TE mode as in equation (30), but with a correction for the finite conductivity of the ground (e.g., *Surkov et al.*, 2005):

$$\left(\frac{J'_v(x_0)}{J_v(x_0)} - i\alpha_p \right) = -\frac{\kappa_a V_{AI}}{\omega} \frac{\kappa_g \cosh \kappa_a d + \kappa_a \sinh \kappa_a d}{\kappa_g \sinh \kappa_a d + \kappa_a \cosh \kappa_a d} \quad (56)$$

where now $\kappa_g = \sqrt{k_\perp^2 - i\omega\mu_0\sigma_g}$ with $\text{Re } \kappa_g > 0$, where σ_g is the ground conductivity. It can be seen here that equation (30) is restored for infinite ground conductivity. For a typical ground conductivity of 10^{-3} mho/m (e.g., *Roble and Tzur*, 1986) and a frequency of 1 Hz, the magnitude of κ_g is about 0.1 km^{-1} , much larger than κ_a for wavelengths the order of a thousand kilometer or more, so the analysis in section 3 is sufficient.

As we noted in section 4, the Hall conductivity of the ionosphere will couple these two modes. Using the full ionospheric jump condition given by equation (31), we can write this as

$$[b_x] = \mu_0 \Sigma_P E_y + \mu_0 \Sigma_H E_x \quad [b_y] = -\mu_0 \Sigma_P E_x + \mu_0 \Sigma_H E_y \quad (57)$$

Note here that we have chosen signs so that the Hall conductance is positive in the northern hemisphere ($\hat{\mathbf{b}} = -\hat{\mathbf{z}}$). Using equation (52) for the shear/TM mode fields and equations (22), (24), and (28) for the fast/TE mode fields, these two conditions become

$$-\frac{i}{V_{AI}} J'_v(x_0) E_{y0} - \frac{i\kappa_a}{\omega} E_{ya} \cosh \kappa_a d = \mu_0 \Sigma_P E_{y0} J_v(x_0) + \mu_0 \Sigma_H E_{x0} J_{-ix_0\epsilon}(x_0) \quad (58)$$

$$\frac{i}{V_{AI}} J'_{-ix_0\epsilon}(x_0) E_{x0} - b_{ya} \cosh \kappa_a d = -\mu_0 \Sigma_P J_{-ix_0\epsilon}(x_0) E_{x0} + \mu_0 \Sigma_H J_v(x_0) E_{y0} \quad (59)$$

Repeating the conditions for continuity of the electric field from equations (29) and (53)

$$E_{ya} \sinh \kappa_a d = E_{y0} J_v(x_0) \quad E_{x0} J_{-ix_0\epsilon}(x_0) = -\frac{i\kappa_a c^2}{\omega} b_{ya} \sinh \kappa_a d \quad (60)$$

we can write the full, coupled dispersion relation for these modes:

$$\left[J'_v(x_0) - \left(i\alpha_p + \frac{\kappa_a V_{AI}}{\omega} \coth \kappa_a d \right) J_v(x_0) \right] \left[J'_{-ix_0\epsilon}(x_0) - \left(i\alpha_p - \frac{\omega V_{AI}}{\kappa_a c^2} \coth \kappa_a d \right) J_{-ix_0\epsilon}(x_0) \right] \quad (61)$$

$$= \alpha_H^2 J_v(x_0) J_{-ix_0\epsilon}(x_0)$$

Note that the hyperbolic cotangent factor in the first factor should be replaced by the right-hand side of equation (56) if the finite ground conductivity is included. Clearly, in the absence of Hall

conductance ($\alpha_H = \mu_0 \Sigma_H V_{Al} \rightarrow 0$), the two factors give the fast/TE mode and the shear/TM mode, respectively. These modes are coupled by the Hall term in general. However, note that in the high conductivity limit ($\alpha_P, \alpha_H \gg 1$), the dispersion relation simply becomes $(\alpha_P^2 + \alpha_H^2) J_v(x_0) J_{-ix_0\epsilon}(x_0) = 0$, and the modes decouple.

Figure 6 shows the effects of the coupling of these two modes. It can be seen that there is a crossover between the dispersive fast/TE mode and the constant frequency shear/TM mode at a wavenumber near 10^{-3} km^{-1} . Thus the lowest frequency mode, for example, starts as the TE mode at long wavelength and crosses over to the IAR mode at smaller wavelength, with the opposite being true of the second lowest mode. The lower panel of the figure shows the damping rates for the first two modes. Note that the TE mode is somewhat lower in damping, and the damping increases as the lowest mode crosses over to the IAR mode. This coupling between the modes gives rise to the excitation of the waveguide mode when the IAR mode is initially excited, as seen in the simulations of *Lysak and Song (2001)* and *Lysak (2004)*.

It should be noted that the coupled dispersion relation, equation (61), although already rather complicated, is not complete. One major approximation was the neglect of the finite conductivity in the atmosphere. In this case, the scale length κ_a should be re-defined as $\kappa_a = \sqrt{k_{\perp}^2 - \omega^2 / c^2 + i\omega\mu_0\sigma_a}$. An approximate model for σ_a would be as an exponential with a value of about 10^{-14} mho/m just above the ground to about 10^{-6} mho/m at the base of the ionosphere, taken as 80 km (e.g., *Roble and Tzur, 1986*). These values imply an exponential scale height of about 4.3 km in the atmosphere. These values imply that the conductivity term in the expression is $8 \times 10^{-14} - 8 \times 10^{-6} \text{ km}^{-2}$ for $\omega = 2\pi \text{ s}^{-1}$, compared to $4 \times 10^{-5} \text{ km}^{-2}$ for a wavelength of 1000 km and $4 \times 10^{-10} \text{ km}^{-2}$ for the light-speed term. Thus, the conductivity correction is not too important for wavelengths of 1000 km or less such as the IAR modes or Pc1 waveguide modes; however, for the purely propagating atmospheric waveguide modes for which $\omega \approx k_{\perp}c$, this conductivity may be important. Using the simple exponential profile described here, the conductivity term is greater than the light speed term above about 45 km. As an example of this effect, *Galejs (1972)* has estimated the Q value of the first Schumann resonance to be in the range 3.8-6.5 using different models of this type.

The other major approximation made in this analysis is the assumption of a vertically incident magnetic field. While this assumption is reasonable for high latitudes, it certainly fails for low latitudes, where the field lines enter the ionosphere obliquely. For oblique dip angles, the degeneracy between the two perpendicular directions is broken, since waves with wave vectors in the latitudinal direction (in the plane of the dipole field) differ from those in the longitudinal direction. *Sciffer and Waters (2002)* and *Sciffer et al. (2004)* have analyzed the reflection and mode conversion of Alfvén and fast mode waves in the presence of oblique magnetic fields. They find a strong dependence on dip angle, especially for longitudinal propagation. One aspect of this interaction is that, while for vertical fields the magnetic fields due to field-aligned and Pedersen currents cancel, this is no longer true for oblique fields. This is due in part to the presence of horizontal field-aligned currents. Thus, in the oblique case the ground magnetic field can be non-zero even in the absence of Hall currents, which is not true for vertical fields. Numerical modeling (*Lysak, 2004*) in a dipole model with oblique fields has confirmed that the coupling between the shear Alfvén modes and fast modes is present in this case.

A final approximation is that of a planar atmosphere, neglecting the curvature of the Earth. While this approximation is reasonable for waves with less than 1000 km perpendicular

wavelength, it must surely fail for the analysis of waves in the atmospheric waveguide at ULF frequencies since waves at frequencies less than the fundamental Schumann resonance (~ 8 Hz) have wavelengths greater than the circumference of the Earth. This does not, however, preclude the presence of transient signal propagation at the speed of light in this waveguide at these frequencies; such waves will not, however, constitute a normal mode of this waveguide. An analysis of these waves in a spherical geometry, which has not yet been published to the best of our knowledge, would shed more light on this subject. It may be noted that *Cummer* (2000) and *Soriano et al.* (2005) have recently developed time-domain models in spherical geometry for atmospheric waves, although their results are restricted to the ELF and VLF frequency ranges. Nevertheless, this technique might be promising for ULF studies in the atmosphere.

It is interesting to note that in addition to being observed at auroral latitudes, signatures of the IAR have been found at low and mid-latitudes (*Polyakov and Rapaport*, 1981; *Belyaev et al.*, 1999; *Bösinger et al.*, 2002, 2004; *Yahnin et al.*, 2003). At these lower latitudes, the excitation of the resonator from externally imposed field-aligned currents is not likely to be effective, so additional mechanisms should be considered. The original observations of *Polyakov and Rapaport* (1981) suggested that thunderstorms could provide an excitation mechanism; this mechanism has been explored in much greater detail by *Surkov et al.* (2005). It has also been suggested that neutral winds might play a role in this excitation (*Surkov et al.*, 2004). In the thunderstorm model, the lightning discharge radiates electric dipole radiation in the TM mode. While the rise of the discharge current takes place in microseconds, the so-called “continuing current” decreases exponentially with time scales the order of 0.1 s (e.g., *Uman*, 1987). Such a quick rise, slow decay exponential has a spectrum that is nearly flat at frequencies below the inverse of the decay time, the order of 10 Hz in this case. Analyzing the radiated wave in a manner similar to that in Section 6 (although they perform this calculation in cylindrical coordinates to analyze the fields of a source localized in horizontal position), *Surkov et al.* (2005) show that the IAR can be excited due to thunderstorms, although the field due to a stochastic distribution of discharges is found to be an order of magnitude below observations; however, nearby thunderstorms can excite stronger fields locally.

7. Conclusions

Understanding the propagation of waves in the strongly inhomogeneous Earth-atmosphere-ionosphere-magnetosphere system is important for the analysis of ULF wave signals observed on the ground as well as with ionospheric radars, particularly at Pc1/Pi1 frequencies the order of 1 Hz. This paper has reviewed the theory of the various waveguides and resonant cavities that can be formed in this system, and showed how they are coupled together. Although, for simplicity, we have restricted the detailed analysis to a slab geometry with vertical magnetic fields, the basic physics of these interactions will persist in the more realistic geometry of the atmosphere.

Although this review has focused on the theoretical aspects of these waveguides and cavities, there are many potential applications of these structures. In the auroral zone, the excitation of waves in the ionospheric Alfvén resonator can lead to the acceleration of auroral electrons (e.g., *Chaston et al.*, 2002a). These waves can also play a role in conductivity variations in the auroral zone leading to a feedback instability (e.g., *Lysak*, 1991; *Lysak and Song*, 2002; *Pokhotelov et al.*, 2002a), which may be a critical ingredient in the formation of narrow auroral arcs (e.g., *Newell et al.*, 1996).

The coupling of magnetospheric ULF waves through the ionosphere to the atmosphere and the ground allows for the observation of these waves by ground magnetometers, even at lower frequencies where the atmospheric modes may be evanescent. At Pc1 frequencies, the fast mode signal can propagate in the ionospheric waveguide and be seen over 1000 km from their source (e.g., *Fraser, 1975; Neudegg et al., 1995*). These waves can be excited by magnetospherically-imposed field-aligned currents carried by the shear Alfvén wave, followed by mode conversion due to the Hall conductivity of the ionosphere (*Yoshikawa and Itonaga, 1996, 2000; Lysak and Song, 2001; Lysak, 2004*). Simultaneous observations of Pc1 and Pi1 signals both in space and on the ground (*Arnoldy et al., 1996, 1998*) confirm this link between magnetospheric and atmospheric fields. Thus, the existence of these waveguide modes, in addition to the coupling caused by the anisotropic conductivity in the ionosphere, is essential for the understanding of ground magnetometer data and its use to understand the field-aligned currents entering the ionosphere.

Consideration of the propagation of waves through the atmospheric waveguide confirms that the TM mode propagates and is not evanescent even at ULF frequencies. However, the large perpendicular wavelength that is required for this mode indicates that a true global waveguide mode cannot be set up at ULF frequencies, where the wavelength would be much larger than the circumference of the Earth. Impulsive events, either externally generated such as the onset of a magnetic storm or internal events such as lightning discharges could excite signals that would propagate at the speed of light and could couple to the ionosphere and magnetosphere.

These considerations suggest that an understanding of the different waveguides and resonant cavities formed by the strong inhomogeneities in the Earth-atmosphere-ionosphere-magnetosphere system is essential both for interpreting the signals observed both on the ground and in space, as well as for propagating information rapidly throughout the system. Further work is clearly needed to describe this signal propagation and the full coupling of this system. Such work would lead to a much better understanding of how the magnetosphere and ionosphere make their presence felt to observers on the ground.

Appendix: Stepwise constant Alfvén speed profile

A number of authors (e.g., *Trakhtengertz and Feldstein, 1984; Fedorov et al., 2001; Pilipenko et al., 2002; Surkov et al., 2005*) have used a stepwise constant profile of the Alfvén speed, where $V_A = V_{AI}$ for $0 \leq z \leq L$ and $V_A = V_{AM}$ for $z > L$. In this case, the solution consists of upgoing and downgoing waves in the lower region and upgoing waves in the upper region. Matching boundary conditions at $z = L$, the solutions can be written as

$$E_x = \begin{cases} \frac{E_M}{2} \left[(1 + \varepsilon) e^{i\omega(z-L)/V_{AI}} + (1 - \varepsilon) e^{-i\omega(z-L)/V_{AI}} \right] & \text{for } 0 \leq z \leq L \\ E_M e^{i\omega(z-L)/V_{AM}} & \text{for } z \geq L \end{cases} \quad (\text{A1})$$

where again we have $\varepsilon = V_{AI} / V_{AM}$.

The relationship between this model and the model presented in section 2 can be seen when we invoke the ionospheric boundary condition given by equations (9) and (10). Inserting the first expression in equation (A1) into this boundary condition, we can write the dispersion relation as (see, e.g., *Surkov et al., 2004*)

$$\frac{1 + \varepsilon - (1 - \varepsilon)e^{2i\omega L/V_{AI}}}{1 + \varepsilon + (1 - \varepsilon)e^{2i\omega L/V_{AI}}} + \alpha_p = 0 \quad (\text{A2})$$

where $\alpha_p = \mu_0 \Sigma_p V_{AI}$. Solving for the phase factor, we find

$$e^{2i\omega L/V_{AI}} = \frac{(1 + \varepsilon)(1 + \alpha_p)}{(1 - \varepsilon)(1 - \alpha_p)} \quad (\text{A3})$$

Note here that while $\varepsilon \ll 1$, α_p can take on any positive value. So for $\alpha_p < 1$, the right-hand side is positive and we can take the log of both sides, recognizing that the logarithm is multiply-valued, to find

$$\frac{2i\omega L}{V_{AI}} = \ln \left[\frac{(1 + \varepsilon)(1 + \alpha_p)}{(1 - \varepsilon)(1 - \alpha_p)} \right] + 2\pi i n \quad (\text{A4})$$

where n is an integer. Rewriting this expression by breaking the ε and α_p parts of the logarithm and expanding for small ε ,

$$\omega_n = \frac{V_{AI}}{L} \left[\pi n - i \left(\varepsilon + \frac{1}{2} \ln \frac{1 + \alpha_p}{1 - \alpha_p} \right) \right] \quad (\text{A5})$$

On the other hand, for the good conductor case, $\alpha_p > 1$, the argument of the logarithm is negative and so a factor of $\ln(-1) = i\pi$ must be factored out. In this case, the frequencies are given by

$$\omega_n = \frac{V_A}{L} \left[\left(n + \frac{1}{2} \right) \pi - i \left(\varepsilon + \frac{1}{2} \ln \frac{\alpha_p + 1}{\alpha_p - 1} \right) \right] \quad (\text{A6})$$

These expressions show that the lowest eigenmode with non-zero frequency is given by $\pi V_{AI} / L$ for a poor conductor and $\pi V_{AI} / 2L$ for a good conductor. In both cases, energy is lost due to leakage out of the top of the resonator (the ε term) as well as dissipation in the ionosphere.

This model is consistent with the exponential model discussed in Section 2 in that the first eigenfrequency decreases from the poor conductivity to the good conductivity case. However, to make the frequencies match, one must take $L = 1.64h$ for low conductivity and $L = 1.31h$ in the high conductivity case. In addition, the eigenfrequencies make a discrete jump at $\alpha_p = 1$ in the step function profile, while the transition is smooth in the exponential case, as can be seen in Figures 3 and 4 of *Lysak* (1991).

Acknowledgements: We thank Yan Song for useful discussions. This work was supported by NASA Grant NAG5-13072 and NSF Grant ATM-0201703.

References:

- Althouse, E. L., and J. R. Davis, Five station observations of Pc1 micropulsation propagation, *J. Geophys. Res.*, **83**, 132, 1978.
- Arnoldy, R. L., M. J. Engebretson, and L. J. Cahill, Bursts of Pc1-2 near the ionospheric footprint of the cusp and their relationship to flux transfer events, *J. Geophys. Res.*, **93**, 1007, 1988.
- Arnoldy, R. L., M. J. Engebretson, J. L. Alford, R. E. Erlandson, and B. J. Anderson, Magnetic impulse events and associated Pc1 bursts at dayside high latitudes, *J. Geophys. Res.*, **101**, 7793, 1996.

- Arnoldy, R. L., J. L. Posch, M. J. Engebretson, H. Fukunishi, and H. J. Singer, Pi1 magnetic pulsations in space and at high latitudes on the ground, *J. Geophys. Res.*, *103*, 23,581, 1998.
- Atkinson, G., Auroral arcs: result of the interaction of a dynamic magnetosphere with the ionosphere, *J. Geophys. Res.* *75*, 4746, 1970.
- Belyaev, P. P., T. Bösinger, S. V. Isaev, and J. Kangas, First evidence at high latitudes for the ionospheric Alfvén resonator, *J. Geophys. Res.*, *104*, 4305, 1999.
- Berthelier, A., J.-C. Cerisier, J.-J. Berthelier, J.-M. Bosqued, and R. A. Kovrazkhin, The electrodynamic signature of short scale field aligned currents, and associated turbulence in the cusp and dayside auroral zone, in *Electromagnetic Coupling in the Polar Clefts and Caps*, P. E. Sandholt and A. Egeland (eds.), Kluwer, Dordrecht, p. 299, 1989.
- Block, L. P., and C.-G. Fälthammar, The role of magnetic-field-aligned electric fields in auroral acceleration, *J. Geophys. Res.*, *95*, 5877, 1990.
- Boehm, M. H., C. W. Carlson, J. P. McFadden, J. H. Clemmons, and F. S. Mozer, High-resolution sounding rocket observations of large-amplitude Alfvén waves, *J. Geophys. Res.*, *95*, 12,157, 1990.
- Bösinger, T., K. Alanko, J. Kangas, H. Opgenoorth, and W. Baumjohann, Correlations between PiB type magnetic micropulsations, auroras, and equivalent current structures during two isolated substorms, *J. Atm. Terr. Phys.*, *43*, 933, 1981.
- Bösinger, T., C. Haldoupis, P. P. Belyaev, M. N. Yakunin, N. V. Semenova, A. G. Demekhov, and V. Angelopoulos, Spectral properties of the ionospheric Alfvén resonator observed at a low-latitude station ($L = 1.3$), *J. Geophys. Res.*, *107*(A10), 1281, doi:10.1029/2001JA005076, 2002.
- Bösinger, T., A. G. Demekhov, and V. Y. Trakhtengerts, Fine structure in ionospheric Alfvén resonator spectra observed at low latitude ($L = 1.3$), *Geophys. Res. Lett.*, *31*, L18802, doi:10.1029/2004GL020777, 2004.
- Chaston, C. C., Carlson, C. W., Ergun, R. E., McFadden, J. P., Alfvén waves, density cavities and electron acceleration observed from the FAST spacecraft, *Physica Scripta*, *T84*, 64-68, 2000.
- Chaston, C. C., J. W. Bonnell, L. M. Peticolas, C. W. Carlson, J. P. McFadden, and R. E. Ergun, Driven Alfvén waves and electron acceleration: A FAST case study, *Geophys. Res. Lett.*, *29*(11), 10.1029/2001GL013842, 2002a.
- Chaston, C. C., J. W. Bonnell, C. W. Carlson, M. Berthomier, L. M. Peticolas, I. Roth, J. P. McFadden, R. E. Ergun, and R. J. Strangeway, Electron acceleration in the ionospheric Alfvén resonator, *J. Geophys. Res.*, *107*(A11), 1413, doi:10.1029/2002JA009272, 2002b.
- Chi, P. J., C. T. Russell, J. Raeder, E. Zesta, K. Yumoto, H. Kawano, K. Kitamura, S. M. Petrinec, V. Angelopoulos, G. Le, and M. B. Moldwin, Propagation of the preliminary reverse impulse of sudden commencements to low latitudes, *J. Geophys. Res.*, *106*, 18,857, 2001.
- Chi, P. J., C. T. Russell, J. Raeder, E. Zesta, K. Yumoto, H. Kawano, K. Kitamura, S. M. Petrinec, V. Angelopoulos, G. Le, and M. B. Moldwin, Reply to comment by T. Kikuchi and T. Araki on “Propagation of the preliminary reverse impulse of sudden commencements to low latitudes,” *J. Geophys. Res.*, *107*(A12), 1474, doi: 10.1029/2002JA009369, 2002.
- Chmyrev, V. M., V. N. Oraevsky, S. V. Bilichenko, N. V. Isaev, G. A. Stanev, D. K. Teodosiev, and S. I. Shkolnikova, The fine structure of intensive small scale electric and magnetic

- fields in the high latitude ionosphere as observed by Intercosmos-Bulgaria-1300 satellite, *Planet. Space Sci.*, 33, 1383, 1985.
- Cummer, S. A., Modeling electromagnetic propagation in the Earth-ionosphere waveguide, *IEEE Trans. Ant. Prop.*, 48, 1420, 2000.
- Erlanson, R. E., L. J. Zanetti, T. A. Potemra, L. P. Block, and G. Holmgren, Viking magnetic and electric field observations of Pc1 waves at high latitudes, *J. Geophys. Res.*, 95, 5941, 1990.
- Fedorov, E., V. Pilipenko, and M. J. Engebretson, ULF wave damping in the auroral acceleration region, *J. Geophys. Res.*, 106(A4), 6203–6212, 2001.
- Fraser, B. J., Ionospheric duct propagation and Pc1 pulsation source, *J. Geophys. Res.*, 80, 2790, 1975.
- Fujita, S., and T. Tamao, Duct propagation of hydromagnetic waves in the upper ionosphere, 1, Electromagnetic field disturbances in high latitudes associated with localized incidence of a shear Alfvén wave, *J. Geophys. Res.*, 93, 14,665, 1988.
- Galejs, J., *Terrestrial Propagation of Long Electromagnetic Waves*, Pergamon Press, Oxford, 1972.
- Grant, I. F., and G. B. Burns, Observations and modeling of correlated PiB magnetic and auroral luminosity pulsations, *J. Geophys. Res.*, 100, 19,387, 1995.
- Greifinger, C., and P. Greifinger, Theory of hydromagnetic propagation in the ionospheric waveguide, *J. Geophys. Res.*, 73, 7473, 1968.
- Greifinger, C., and P. Greifinger, Wave guide propagation of micropulsations out of the plane of the geomagnetic meridian, *J. Geophys. Res.*, 78, 4611, 1973.
- Grzesiak, M., Ionospheric Alfvén resonator as seen by Freja satellite, *Geophys. Res. Lett.*, 27, 923, 2000.
- Gurnett, D. A., R. L. Huff, J. D. Menietti, J. L. Burch, J. D. Winningham, and S. D. Shawhan, Correlated low-frequency electric and magnetic noise along auroral field lines, *J. Geophys. Res.*, 89, 8971, 1984.
- Hansen, H. D., B. J. Fraser, F. W. Menk, Y.-D. Hu, P. T. Newell, C.-I. Meng, and R. J. Morris, High-latitude Pc1 bursts arising in the dayside boundary layer region, *J. Geophys. Res.*, 97, 3993, 1992.
- Heacock, R. R., Two subtypes of type Pi micropulsations, *J. Geophys. Res.*, 72, 3905, 1967.
- Hirano, Y., H. Fukunishi, R. Kataoka, T. Hasunuma, T. Nagatsuma, W. Miyake, and A. Matsuoka, Evidence for the resonator of inertial Alfvén waves in the cusp topside ionosphere, *J. Geophys. Res.*, 110, A07218, doi: 10.1029/2003JA010329, 2005.
- Hughes, W. J., The effect of the atmosphere and ionosphere on long period magnetospheric micropulsations, *Planet. Space Sci.*, 22, 1157, 1974.
- Iyemori, T., and K. Hayashi, Pc1 micropulsations observed by Magsat in the ionospheric F region, *J. Geophys. Res.*, 94, 93, 1989.
- Jackson, J. D., *Classical Electrodynamics*, Third Edition, Wiley, New York, 1999.
- Jacobs, J. A., and T. Watanabe, Propagation of hydromagnetic waves in the lower exosphere and the origin of short period geomagnetic pulsations, *J. Atmos. Terr. Phys.*, 24, 413, 1962.
- Kelley, M. C., *The Earth's Ionosphere*, Academic Press, Inc., 1989.
- Kikuchi, T., and T. Araki, Transient response of uniform ionosphere and preliminary reverse impulse of geomagnetic storm sudden commencements, *J. Atmos. Terr. Phys.*, 41, 917, 1979a.

- Kikuchi, T., and T. Araki, Horizontal transmission of the polar electric field to the equator, *J. Atmos. Terr. Phys.*, *41*, 927, 1979b.
- Kikuchi, T., and T. Araki, Comment on "Propagation of the preliminary reverse impulse of sudden commencements to low latitudes," by P. J. Chi et al., *J. Geophys. Res.*, *107*(A12), 1473, doi: 10.1029/2001JA009220, 2002.
- Knudsen, D. J., M. C. Kelley, G. D. Earle, J. F. Vickrey, and M. Boehm, Distinguishing Alfvén waves from quasi-static field structures associated with discrete aurora: sounding rocket and HILAT measurements, *Geophys. Res. Lett.*, *17*, 921, 1990.
- Knudsen, D. J., M. C. Kelley, and J. F. Vickrey, Alfvén waves in the auroral ionosphere: a numerical model compared with measurements, *J. Geophys. Res.*, *97*, 77, 1992.
- Koskinen, H. E. J., R. E. Lopez, R. J. Pellinen, T. I. Pulkkinen, D. N. Baker, and T. Bösinger, Pseudobreakup and substorm growth phase in the ionosphere and magnetosphere, *J. Geophys. Res.*, *98*, 5801, 1993.
- Lysak, R. L., Coupling of the dynamic ionosphere to auroral flux tubes, *J. Geophys. Res.*, *91*, 7047, 1986.
- Lysak, R. L., Theory of auroral zone PiB pulsation spectra, *J. Geophys. Res.*, *93*, 5942, 1988.
- Lysak, R. L., Feedback instability of the ionospheric resonant cavity, *J. Geophys. Res.*, *96*, 1553, 1991.
- Lysak, R. L., Generalized model of the ionospheric Alfvén resonator, in *Auroral Plasma Dynamics*, R. L. Lysak (ed.), AGU Monograph 80, p. 121, 1993.
- Lysak, R. L., Propagation of Alfvén waves through the ionosphere: Dependence on ionospheric parameters, *J. Geophys. Res.*, *104*, 10,017, 1999.
- Lysak, R. L., Magnetosphere-ionosphere coupling by Alfvén waves at midlatitudes, *J. Geophys. Res.*, *109*, A07201, doi:10.1029/2004JA010454, 2004.
- Lysak, R. L., and Y. Song, A three-dimensional model of the propagation of Alfvén waves through the auroral ionosphere: First results, *Adv. Space Research*, *28*, 813, 2001.
- Lysak, R. L., and Y. Song, Energetics of the ionospheric feedback interaction, *J. Geophys. Res.*, *107*(A8), 10.1029/2001JA000308, 2002.
- Lysak, R. L., and Y. Song, Magnetosphere-ionosphere coupling by Alfvén waves: Beyond current continuity, in press, *Adv. Space Res.*, 2005.
- Manchester, R. N., Correlation of Pc1 micropulsations at spaced stations, *J. Geophys. Res.*, *73*, 3549, 1968.
- Marklund, G. T., L. G. Blomberg, C.-G. Fälthammar, R. E. Erlandson, and T. A. Potemra, Signatures of the high-altitude polar cusp and dayside aurora regions as seen by the Viking electric field experiment, *J. Geophys. Res.*, *95*, 5767, 1990.
- Neudegg, D. A., B. J. Fraser, F. W. Menk, H. J. Hansen, G. B. Burns, R. J. Morris, and M. J. Underwood, Source and velocities of Pc1-2 ULF waves at high latitudes, *Geophys. Res. Lett.*, *22*, 2965, 1995.
- Newell, P. T., C.-I. Meng, and K. M. Lyons, Suppression of discrete aurora by sunlight, *Nature*, *381*, 766, 1996.
- Pilipenko, V. A., E. N. Fedorov, and M. J. Engebretson, Alfvén resonator in the topside ionosphere beneath the auroral acceleration region, *J. Geophys. Res.*, *107*(A9), 1257, doi:10.1029/2002JA009282, 2002.
- Pilipenko, V., E. Fedorov, M. J. Engebretson, and K. Yumoto, Energy budget of Alfvén wave interactions with the auroral acceleration region, *J. Geophys. Res.*, *109*, A10204, doi:10.1029/2004JA010440, 2004.

- Pokhotelov, D., W. Lotko, and A. V. Streltsov, Harmonic structure of field line eigenmodes generated by ionospheric feedback instability, *J. Geophys. Res.*, *107*(A11), 1363, doi:10.1029/2001JA000134, 2002a .
- Pokhotelov, D., W. Lotko, and A. V. Streltsov, Effects of the seasonal asymmetry in ionospheric Pedersen conductance on the appearance of discrete aurora, *Geophys. Res. Lett.*, *29*(10), doi:10.1029/2001GL014010, 2002b.
- Pokhotelov, O., D. Pokhotelov, A. Streltsov, V. Khrushev, and M. Parrot, Dispersive ionospheric Alfvén resonator, *J. Geophys. Res.*, *105*, 7737, 2000.
- Polyakov, S. V., and V. O. Rapoport, Ionospheric Alfvén resonator, *Geomag. Aeronomy*, *21*, 816, 1981.
- Popecki, M., R. Arnoldy, M. J. Engebretson, and L. J. Cahill, High-latitude ground observations of Pc1/2 micropulsations, *J. Geophys. Res.*, *98*, 21,481, 1993.
- Potemra, T. A., R. E. Erlandson, L. J. Zanetti, R. L. Arnoldy, J. Woch, and E. Friis-Christensen, The dynamic cusp, *J. Geophys. Res.*, *97*, 2835, 1992.
- Roble, R. G., and I. Tzur, The global atmosphere-electrical circuit, in *The Earth's Electrical Environment*, E. P. Krider and R. G. Roble (eds.), National Academy Press, Washington, DC, 1986.
- Sato, T., A theory of quiet auroral arcs, *J. Geophys. Res.*, *83*, 1042, 1978.
- Schumann, W. O., On the radiation free self oscillations of a conducting sphere, which is surrounded by an air layer and an ionospheric shell, *Z. Naturforsch.*, *72*, 149, 1952.
- Sciffer, M. D., and C. L. Waters, Propagation of ULF waves through the ionosphere: Analytic solutions for oblique magnetic fields, *J. Geophys. Res.*, *107*(A10), 1297, doi: 10.1029/2001JA000184, 2002.
- Sciffer, M. D., C. L. Waters, and F. W. Menk, Propagation of ULF waves through the ionosphere: Inductive effect for oblique magnetic fields, *Ann. Geophys.*, *22*, 1155, 2004.
- Soriano, A., E. A. Navarro, D. L. Paul, J. A. Porti, J. A. Morente, and I. J. Craddock, Finite difference time domain simulation of the Earth-ionosphere resonant cavity: Schumann resonances, *IEEE Trans. Ant. Prop.*, *53*, 1535, 2005.
- Surkov, V. V., O. A. Pokhotelov, M. Parrot, E. N. Fedorov, and M. Hayakawa, Excitation of the ionospheric resonance cavity by neutral winds at middle latitudes, *Ann. Geophys.*, *22*, 3877, 2004.
- Surkov, V. V., O. A. Molchanov, M. Hayakawa, and E. N. Fedorov, Excitation of the ionospheric resonance cavity by thunderstorms, *J. Geophys. Res.*, *110*, A04308, doi: 10.1029/2004JA010850, 2005.
- Tamao, T., The structure of three-dimensional hydromagnetic waves in a uniform cold plasma, *J. Geomag. Geoelectr.*, *18*, 89, 1964.
- Tanaka, H., Y. Saito, K. Asamura, S. Ishii, and T. Mukai, High time resolution measurement of multiple electron precipitations with energy-time dispersion in high-latitude part of the cusp region, *J. Geophys. Res.*, *110*, A07204, doi:10.1029/2004JA010664, 2005.
- Temerin, M., C. Cattell, R. Lysak, M. Hudson, R. B. Torbert, F. S. Mozer, R. D. Sharp, and P. M. Kintner, The small scale structure of electrostatic shocks, *J. Geophys. Res.*, *86*, 11,278, 1981.
- Thompson, B. J., and R. L. Lysak, Electron acceleration by inertial Alfvén waves, *J. Geophys. Res.*, *101*, 5359, 1996.
- Trakhtengertz, V. Yu., and A. Ya. Feldstein, Quiet auroral arcs: ionospheric effect of magnetospheric convection stratification, *Planet. Space Sci.*, *32*, 127, 1984.

- Trakhtengertz, V. Yu., and A. Ya. Feldstein, Turbulent Alfvén boundary layer in the polar ionosphere, I, Excitation conditions and energetics, *J. Geophys. Res.*, *96*, 19,363, 1991.
- Uman, M. A., *The Lightning Discharge*, Academic Press, Orlando, 1987.
- Volwerk, M., P. Louarn, T. Chust, A. Roux, and H. de Feraudy, Solitary kinetic Alfvén waves: A study of the Poynting flux, *J. Geophys. Res.*, *101*, 13,335, 1996.
- Yahnin, A. G., N. V. Semenova, A. A. Ostapenko, J. Kangas, J. Manninen, and T. Turunen, Morphology of the spectral resonance structure of the electromagnetic background noise in the range of 0.1-4.0 Hz at L=5.2, *Ann. Geophys.*, *21*, 779, 2003.
- Yahnina, T. A., A. G. Yahnin, J. Kangas, and J. Manninen, Proton precipitation related to Pc1 pulsations, *Geophys. Res. Lett.*, *27*, 3575, 2000.
- Yoshikawa, A., How does the ionospheric rotational Hall Current absorb the increasing energy from the field-aligned current system?, *Geophys. Res. Lett.*, *29* (7), 1133, doi: 10.1029/2001GL014125, 2002.
- Yoshikawa, A., and M. Itonaga, Reflection of shear Alfvén waves at the inductive ionosphere, *Geophys. Res. Lett.*, *23*, 101, 1996.
- Yoshikawa, A., and M. Itonaga, The nature of reflection and mode conversion of MHD waves in the inductive ionosphere: Multistep mode conversion between divergent and rotational electric fields, *J. Geophys. Res.*, *105*, 10,565, 2000.
- Yoshikawa, A., M. Itonaga, S. Fujita, H. Nakata, and K. Yumoto, Eigenmode analysis of field line oscillations interacting with the ionosphere-atmosphere-solid earth electromagnetic coupled system, *J. Geophys. Res.*, *104*, 28,437, 1999.
- Yoshikawa, A., Y. Obana, M. Shinohara, M. Itonaga, and K. Yumoto, Hall-induced inductive shielding effect on geomagnetic pulsations, *Geophys. Res. Lett.*, *29*(8), 1266, doi: 10.1029/2001GL013610, 2002.

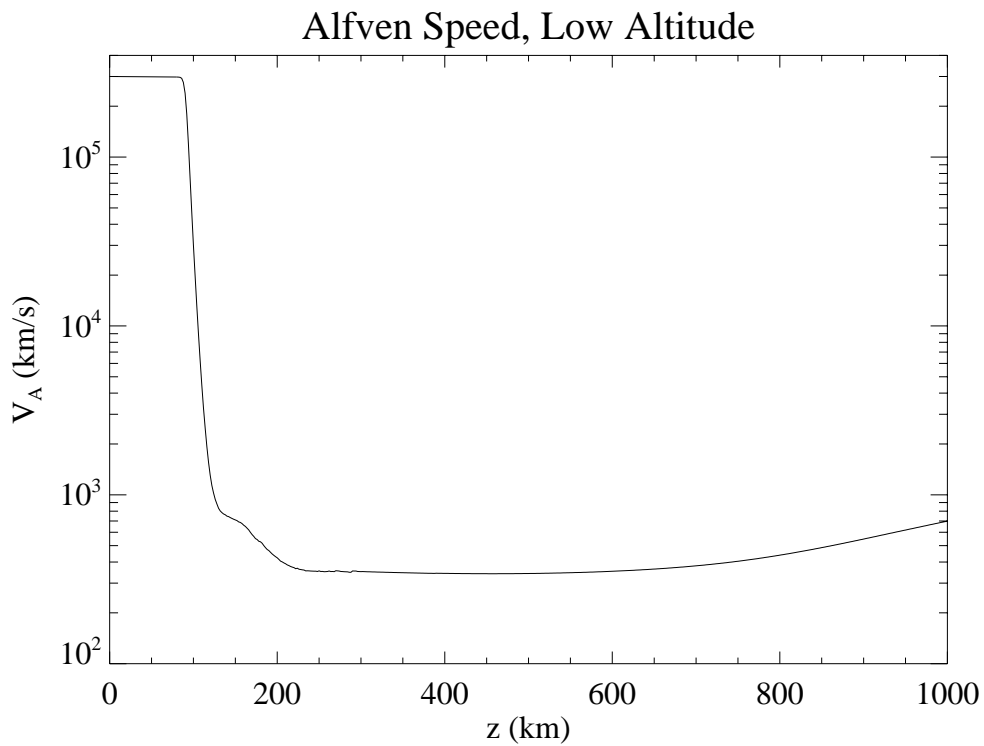
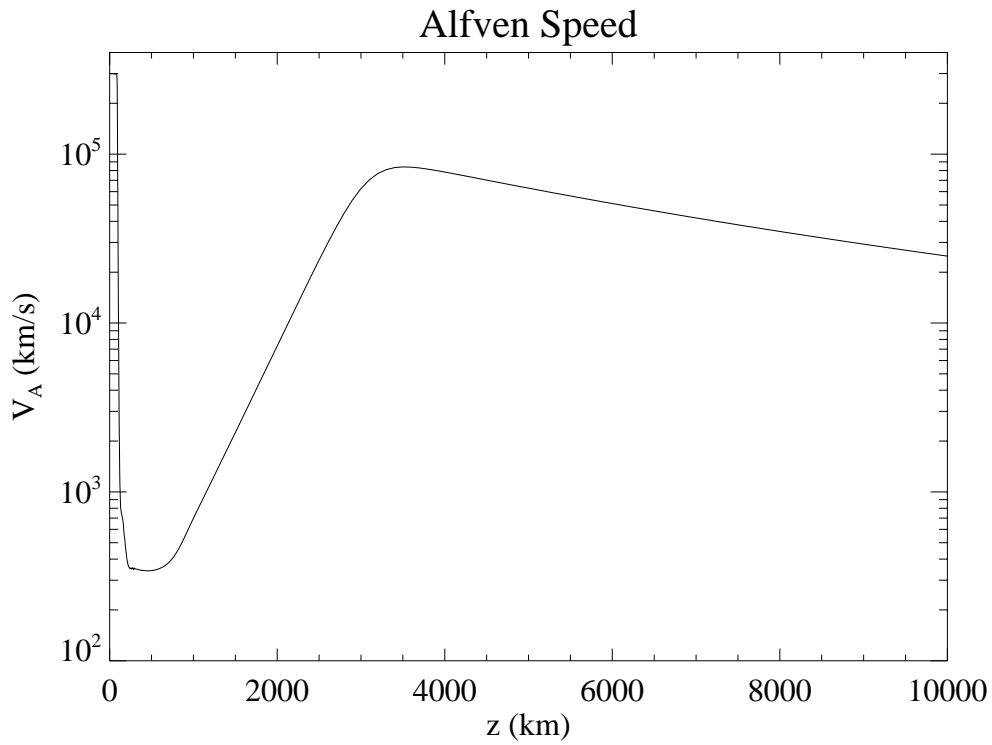


Figure 1. Profile of the Alfvén speed for parameters based on the MSIS and IRI models. Top panel shows up to 10,000 km altitude; bottom panel up to 1000 km.

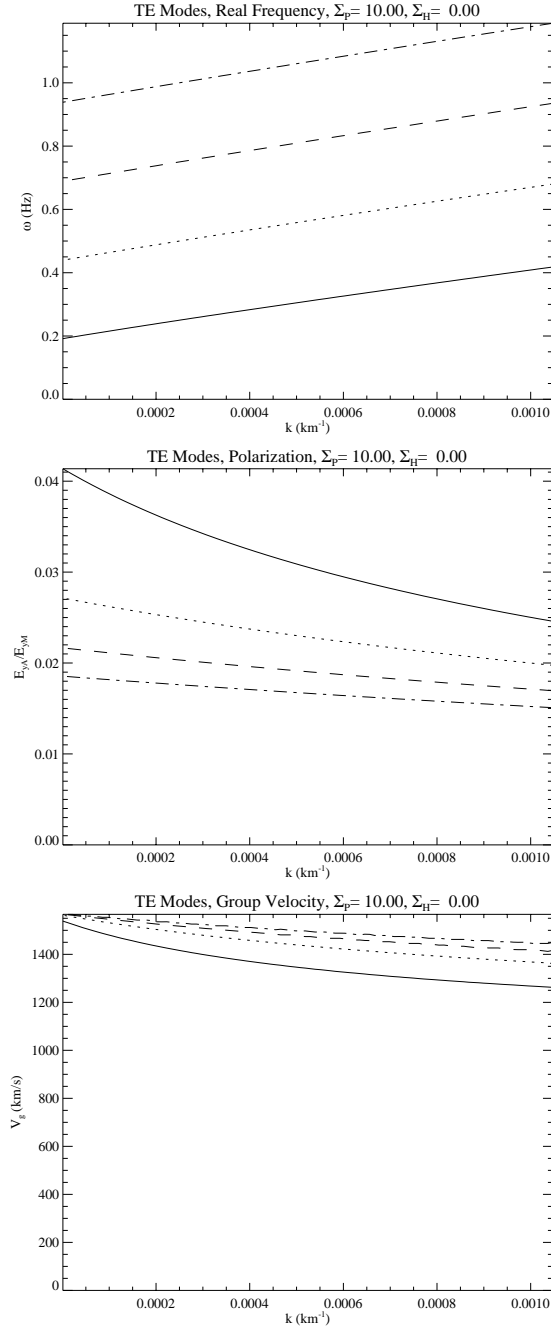


Figure 2. Dispersion relation for the first four fast/TE coupled modes for $\Sigma_P = 10$ mho. Top panel: Real frequency. Middle panel: Ratio of maximum atmospheric to ionospheric electric field. Bottom panel: Group velocity. Other parameters assumed are 1000 km/s for the ionospheric Alfvén speed, 100,000 km/s for the magnetospheric Alfvén speed, and 1000 km for the topside ionosphere scale height.

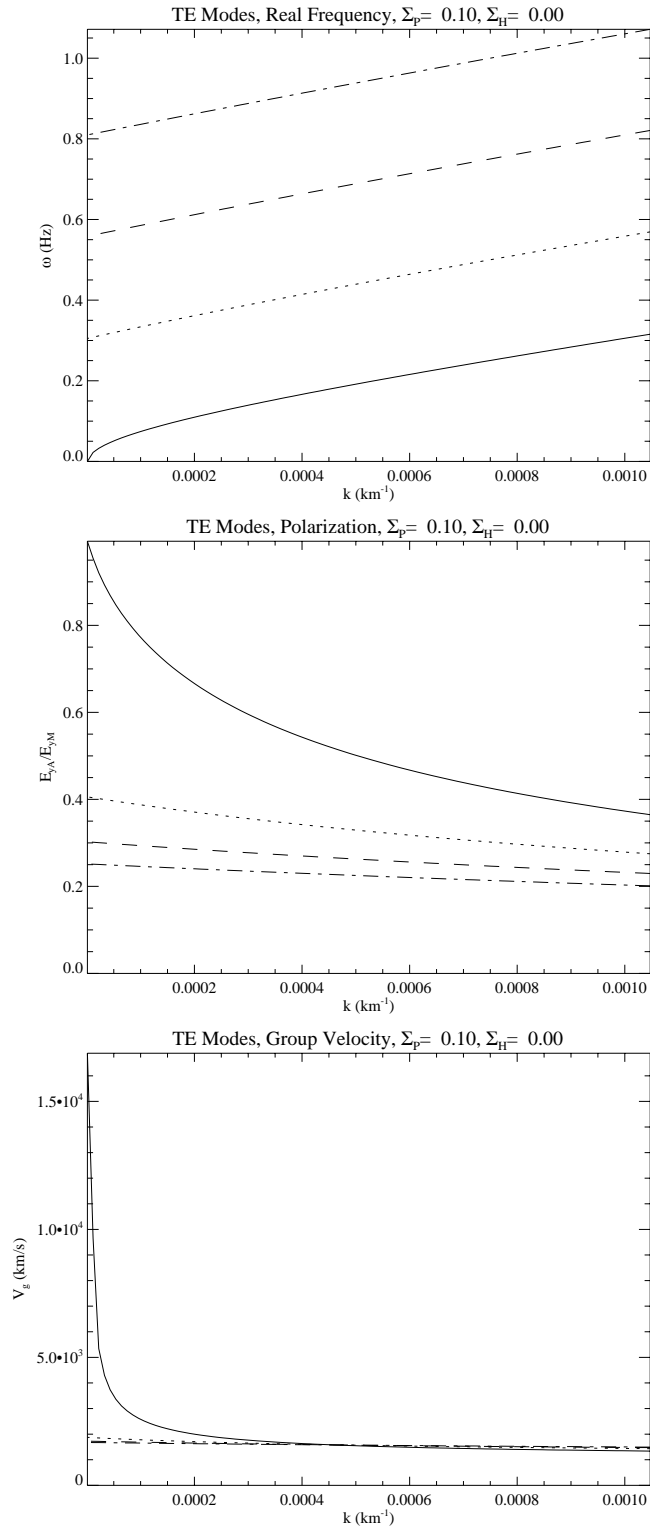


Figure 3. Same as Figure 2 for an ionospheric Pedersen conductance of 0.1 mho.

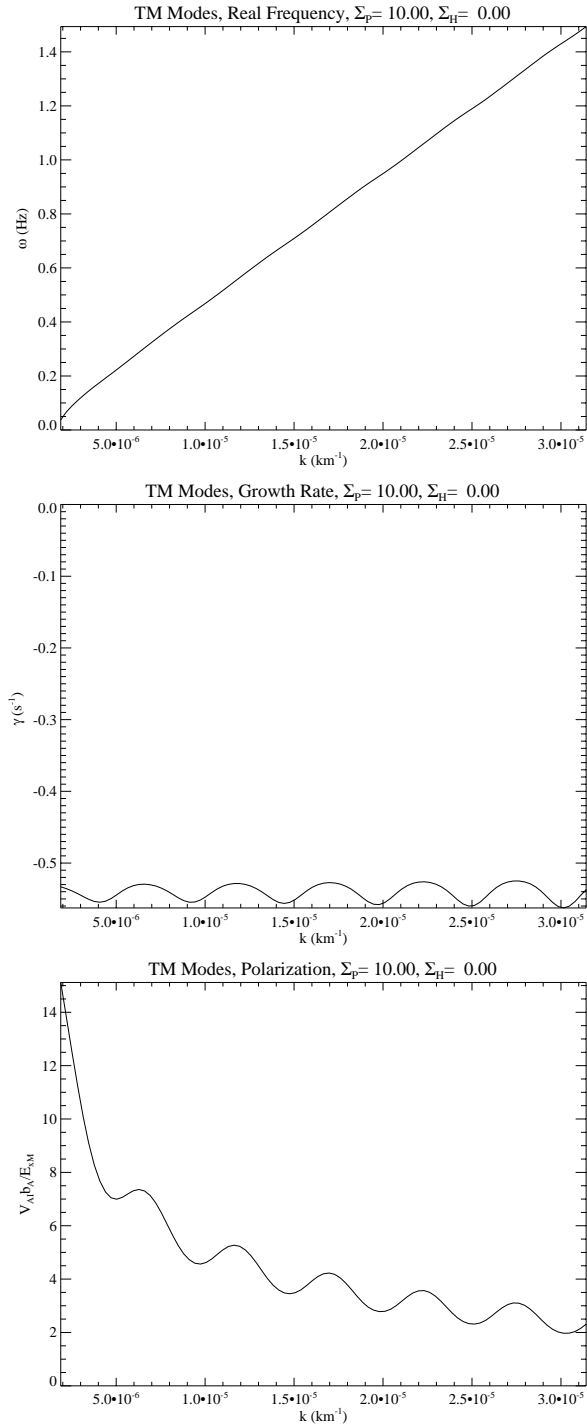


Figure 4. Dispersion characteristics of the atmospheric waveguide mode for $\Sigma_p = 10$ mho.. Top panel: real frequency. Middle panel: growth rate. Bottom panel: Ratio of the atmospheric magnetic field times the ionospheric Alfvén speed to the ionospheric electric field. Other parameters are as in Figure 2.

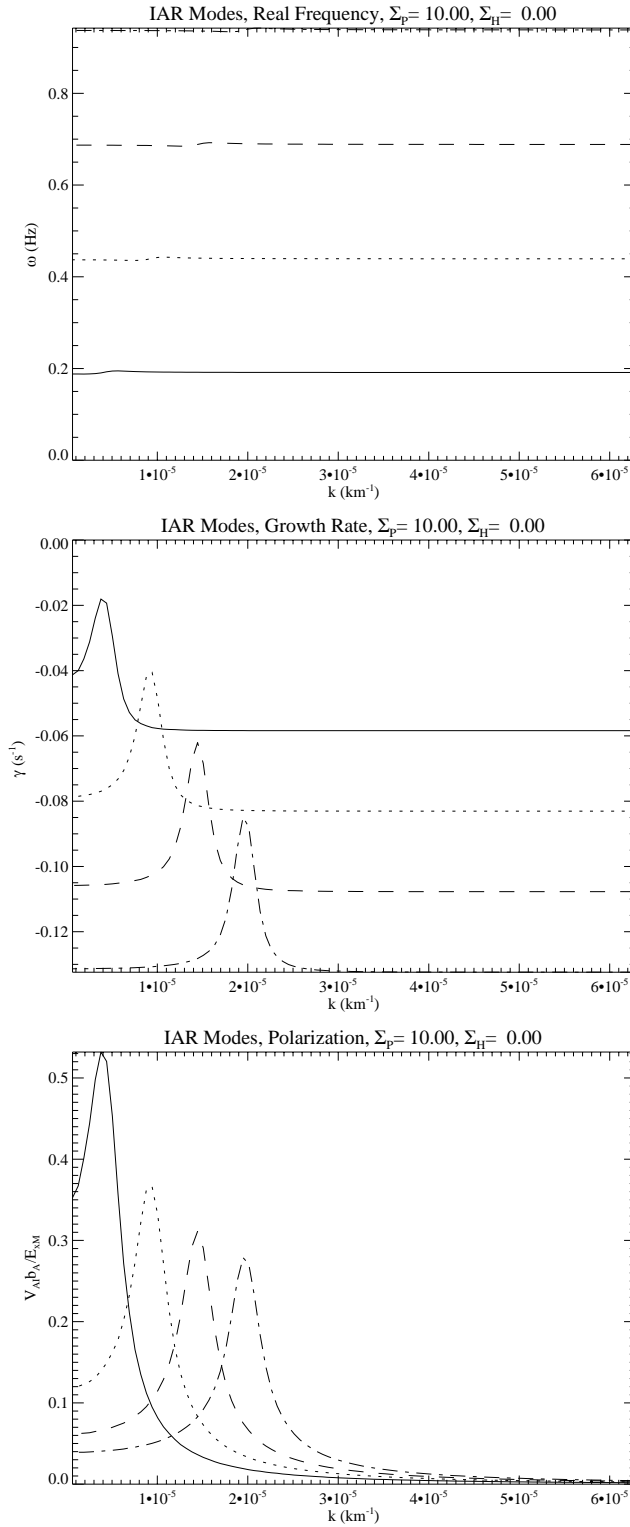


Figure 5. Dispersion characteristics of the ionospheric Alfvén resonator coupled to the atmospheric waveguide. Format and assumed parameters are as in Figure 4.

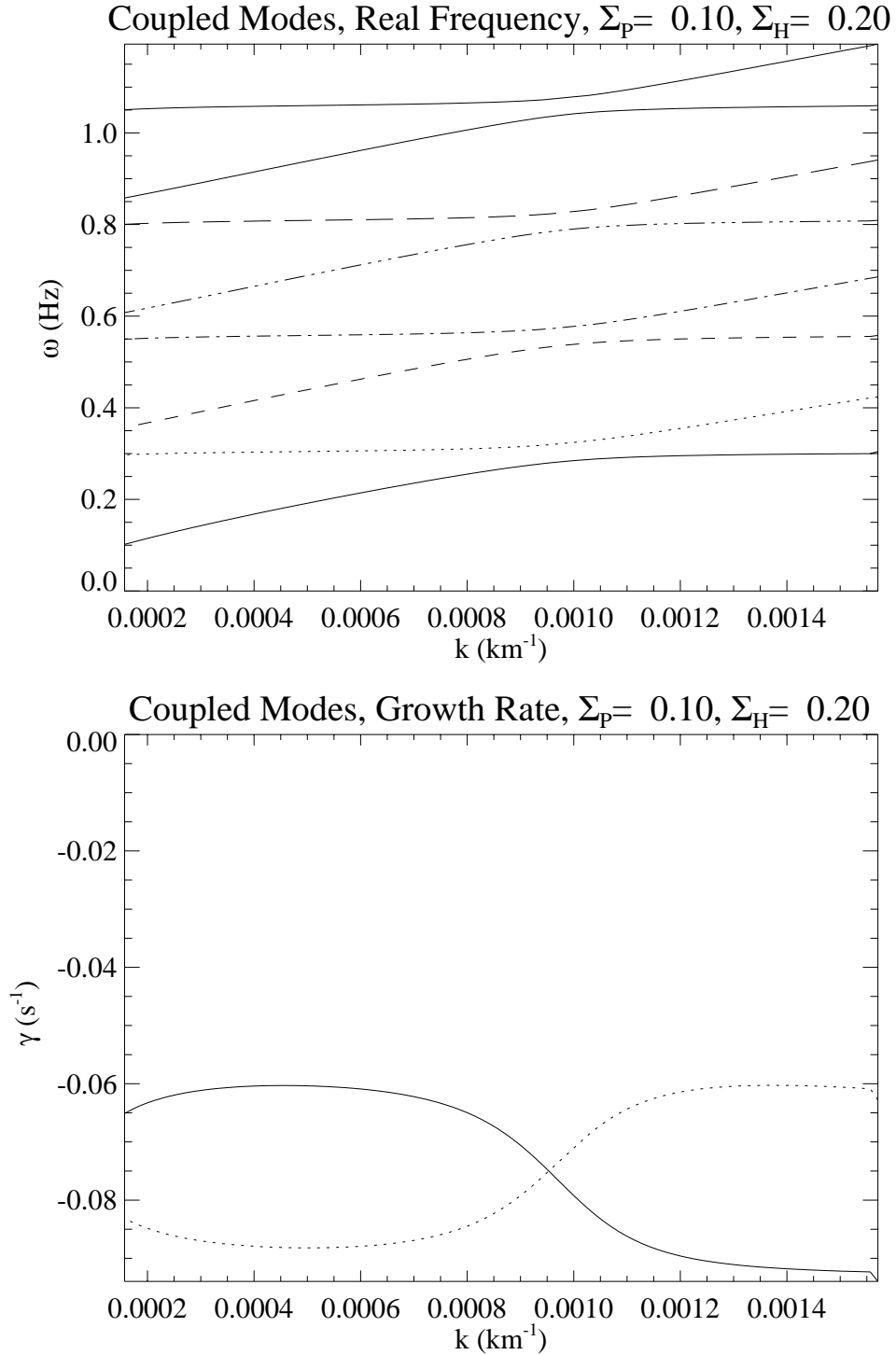


Figure 6. Dispersion characteristics of the fast and shear Alfvén modes coupled by the Hall conductance for $\Sigma_P = 0.1$ mho and $\Sigma_H = 0.2$ mho. Other parameters are the same as in the other figures. Top panel: Real frequency. Bottom panel: Growth (damping) rate for the lowest two modes.